Modeling Hysteresis Effects in Boiler Components

MSc Thesis

Faculty of Applied Sciences
Sustainable Energy Technology

V. Stathis
July 2013

TU Delft Delft University of Technology

Challenge the future

Modeling Hysteresis Effects in Boiler Components

MASTER OF SCIENCE THESIS

For the degree of Master of Science in Sustainable Energy Technology at Delft University of Technology

V. Stathis

July 16, 2013

DELFT UNIVERSITY OF TECHNOLOGY

DEPARTMENT OF

PROCESS AND ENERGY (PE)

The undersigned hereby certify that they have read and recommend to the Faculty of Applied Sciences for acceptance a thesis entitled

MODELING HYSTERESIS EFFECTS IN BOILER COMPONENTS

by

V. STATHIS

in partial fulfillment of the requirements for the degree of

MASTER OF SCIENCE SUSTAINABLE ENERGY TECHNOLOGY

Dated: July 16, 2013

Supervisor(s):

Prof. ir. B.J. Boersma

Dr. ir. R. Pecnik

ir. S. Z. Boksteen

Dr. A. Gangoli Rao

Reader (s):

ir. D.J. van der Vecht

Abstract

The introduction of renewable energy technologies such as wind and solar energy in the electricity market cause the increase of load variations and rapid load changes of large Gas Turbine Combined Cycle (GTCC) power plants. This leads to the evolution of extra thermal stresses in critical parts of the plant such as the boiler. The present study is focused on the development of simulation models that are able to calculate the evolution of thermomechanical stresses in critical components of the boiler. Such models can be useful in analyzing and estimating the fatigue lifetime of boiler components and therefore can be helpful in reducing maintenance costs.

This report consists of two parts; In the first part a literature review is presented, along with a fatigue assessment methodology according to the EN 12952-3 standard. Then the mathematical model that has been developed is described.

In the second part, the proposed methodology is applied in an existing GTCC power plant using online data. The simulation is focused on the high pressure steam drum of the unit and the results show that the component experiences a cycling loading in daily operation. By implementing a fatigue cycle counting technique based on the rainflow algorithm, the amplitude and mean stress of each identified cycle are determined. Finally, using these outcomes the fatigue lifetime of the component can be estimated.

Various simulation scenarios are considered in this study. These include start-up / shut down of the plant, load change and daily operation. According to the simulation results the most severe situation is the start-up where the highest stress amplitudes are observed. Nevertheless, the calculated stresses are well below the yield stress of the material, leading to a theoretically infinite fatigue lifetime.

The implementation of the simulation models to the other components of the boiler, such as the superheater headers, can give a better insight to the consequences of cycling modern GTCC power plants.

Acknowledgements

In this section I would like to express my acknowledgements to those who helped me to complete this project with success.

Firstly, I would like to thank Mr. B.J. Boersma for giving me the chance to work on this interesting subject. Even though he is a very busy person he always had some time for me to discuss and give his advice for the project.

Of course, I would like to thank my daily supervisor Mr. S.Z. Boksteen for his guidance throughout this project. Also, I would like to thank Mr. R. Pecnik for his feedback in the modeling process.

It is important to mention that the work in this thesis was supported by GDF Suez. Their cooperation and assistance is hereby gratefully appreciated. Moreover, a special thanks goes to Mr. M. Lahoye for his guidance and cooperation especially at the beginning of this project.

Last but not least, I would like to thank my parents for their support throughout all these years of my studies. Without them I wouldn't achieve all of my goals.

Delft University of Technology V. Stathis
July 16, 2013

Table of Contents

List of Figures

List of Tables

Nomenclature

Abbreviations

CCS	Carbon Capture and Storage
EFOR	Equivalent Forced Outage Rates
FAC	Flow Accelerated Corrosion
FEA	Finite Element Analysis
GFT	Green's Function Technique
GT	Gas Turbine
GTCC	Gas Turbine Combined Cycle
HP	High Pressure
HP Drum	High Pressure Drum
HPSH	High Pressure Superheater
HRSG	Heat Recovery Steam Generator
IP	Intermediate Pressure
LP	Low Pressure
RHTR	Reheater

Latin Symbols

B	Biot number for heat-transfer (-)
c	Fatigue ductility exponent (-)
C	Fatigue damage ratio (-)
D	Thermal diffusivity (mm^2/s)
E	Modulus of elasticity (MPa)
H	The convective heat transfer coefficient (W/m^2K)
K	Heat conductivity (W/mK)
L	Wall thickness (mm)
n	Number of cycles at stress σ (-)
N	Number of cycles to failure at stress σ (-)
p	Pressure (MPa)
r	Radius (mm)
T	Temperature (°C)
t	Time (s)

Greek Symbols

α	Coefficient of linear thermal expansion (K^{-1})
Δσ/2	Fatigue cycle peak amplitude (MPa)
ε	Strain (mm)
ν	Poisson's ratio (-)
σ	Stress (MPa)

τ	Fatigue cycle period (s)

Subscripts

f	Fluid
i	Inner
m	Mean
o	Outer
r	Radial direction
t	Tangential direction
z	Axial direction
th	Thermal
0	Initial

1. INTRODUCTION

In the introductory part a brief explanation of the motivation for this study is given. The changing aspects of the current and future energy market are discussed and the impacts of this change are mentioned. Then various methods of investigating the transient behavior of critical components in a utility boiler are discussed. Finally, the approach for the solution of the problem is explained for the reader to provide a clear view of the strategy that is followed.

1.1. Future Electricity Markets

Electricity demand from individual power plants is increasingly fluctuating due to factors related to gas and electricity prices as well as a more volatile power generation pattern particularly as the share of renewable, such as wind derived energy is growing faster. Power generation from wind is variable over time, due to the fluctuations of wind speed. Also, wind power output alters the shape of the net load to be satisfied with conventional thermal power generation, therefore changing the traditional way to schedule the thermal portfolio. Peaks of thermal power production no longer occur when demand is highest. Additionally, wind production may result in such a low value of net demand (mostly at night) that will force a large number of thermal units to shut down and to have then start-up just a few hours later [1].

Figure 1-1 shows the results of a survey done to forecast the future energy market in Great Britain [2]. The main effect of the increase of renewables share in the electricity market, is a more irregular power generation pattern which will inevitably have an effect on maintenance of the plant, both increasing its cost and reducing the life of the plant.

Moreover, deregulation and consequent merchant power have made it important for thermal power plants to supply electrical power to the grid as and when needed with minimum notice.

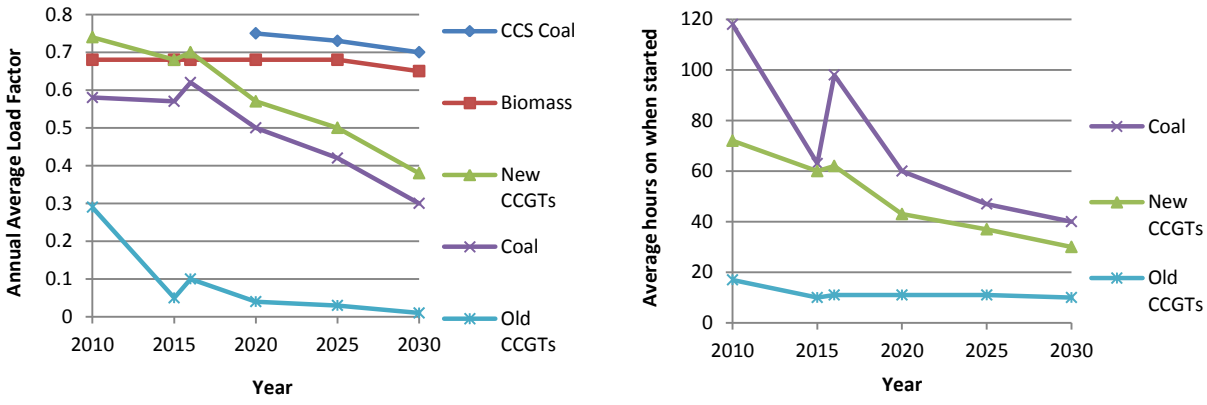

***Figure 1-1**: Annual load factors and average hours when started (Source: [2])*

Hence, there is a high demand for reducing start-up and shut down costs in power plants. Further reasons directly related to start-up costs of power plants are fuel, auxiliary load and auxiliary steam savings resulting from shorter start-up procedures which, in addition, increase the environmental compatibility of the process due to minimized overall emissions [3].

Power plants are also forced to run on partial loads. Even units originally designed for base load operation are eventually forced to cycle like the new, more efficient power plants that have been build recently. As a result, power plant operators have to deal with increasing load variations and rapid load changes [4].

1.2. Implications of Cycling Operation

The transition of the electricity markets would have some implications in new, as well as, existing power plants. Lefton et al. [5] summarized the impacts of fossil power plant cycling operation:

- Significant increase in equivalent forced outage rate (EFOR).
- Additional capital and maintenance expenditures.
- Increase fatigue-related and creep-related wear and tear.

The present study aims to investigate the fatigue-related wear and tear of boiler components as a consequence of the increased cycling of thermal power plants.

Definitions of cycling have varied from on/off starts (normally defined as hot, warm and cold starts) and two-shifting to loading cycling and high frequency load variations. Two-shifting means that the unit is operating in two shifts, one full-load and one part-load. Cycling typically increases fatigue-related wear and tear. In operation of power plants, changes in load variation result in the evolution of thermomechanical stresses especially in critical parts of boiler components. These components have a relative thick wall and experience high temperature and pressure changes (e.g. steam drums, superheater and reheater tubing and headers, water wall/evaporator tubing). The developed stresses must not exceed pre-specified values, depending on the material used and the current pressure and temperature values. In order to minimize thermal losses and moreover to be flexible, it is desirable to operate as close to these limits as possible [6].

Generally speaking, manufacturers use very safe limits to guarantee the safe operation of the components. However, failures in power plants caused by frequent cycling can still occur [7]. In boilers, in the superheater section, damage to tubing is usually caused by overheating which results from low or no flow of cooling steam through the tubes during start-up or part-load operation. Damage to superheater tubing is usually evident by severe bowing and thermal distortion due to overheating damage of tubes fully exposed in the gas path. Also, superheater tube damage can result from condensate, and stagnate or reverse steam flows during start-up. Similar overheating damage often occurs in reheater tubing too. In heat recovery steam generators (HRSGs), the typical cycling problems can be traced back to superheater and reheater drains that fail to clear accumulated condensate. Flow-accelerated corrosion (FAC) in the low-

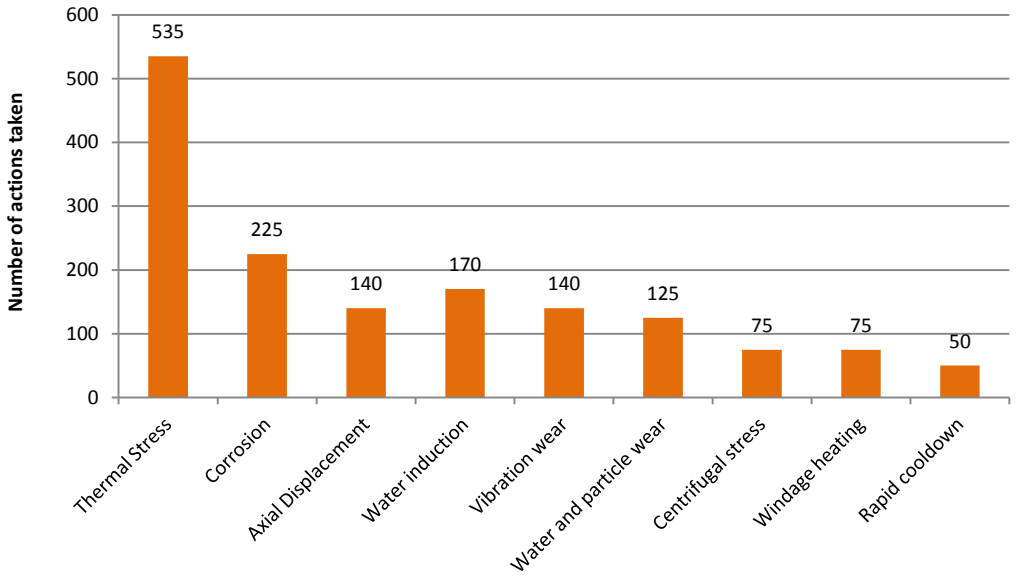

Figure 1-2: *Common problems in cycling plants (Source: [7]).*

pressure evaporator and failure of feedwater heaters from thermal shock and FAC also are often found [7].

Figure 1-2 shows the results of a survey for 215 steam plants which found to have many common equipment problems. As it can be seen, thermal stress is a major problem which is very common in steam power plants. The problem of fatigue due to high thermal stresses during temperature transients has not been regarded as major one [8]. However, as already mentioned, the increasing prevalence of a two-shifting mode means that a power plant experiences many more start-up and shut down cycles than it has previously been the case.

It is therefore of great importance to determine and calculate the evolution of stress in critical boiler components, in order to operate in an effective but also reliable manner for the complete system. Today's analytical techniques to assess transient behavior and the associated stresses and fatigue damage can be used in combination with off-line analysis and on-line monitoring to better quantify the consequences of this flexible operation. In addition, such analysis and monitoring can provide valuable insights into weak-links or bottlenecks in the system that can limit rates of response or hamper the ability to continuously operate at particular load points [9].

This study will focus on the Heat Recovery Steam Generator (HRSG) of an existing Gas Turbine Combined Cycle (GTCC) plant. The HRSG is after the gas turbine, one of the most important contributors to the cycling performance capabilities of a combined cycle power plant. To meet these challenges, the HRSG must be capable of rapid load transients and prolonged periods of operation at low loads (providing spinning reserve). As generally recognized nowadays, the cycling criterion is an integral part of the HRSG design.

1.3. Literature Review

As already mentioned, cycling operation involves rapid increases and decreases in process temperatures, which create significant thermal stress on pressure boundaries. A few important material damage mechanisms are responsible for the majority of the impacts caused by operating power plants in flexible modes. The severity of the impact of these mechanisms can be mitigated to a certain extent through improved plant operation and process controls, but it is impossible to completely eliminate the reduction in major component life by flexible operation.

Thermal fatigue is a phenomenon which can produce cracking in thick-walled boiler components. In principal, thermal fatigue damage occurs due to thermal transients and pressure inside the critical components. The stresses due to pressure (mechanical stresses) can be calculated by factoring the measured pressure in the critical components. On the other hand, the stresses due to thermal transients (thermal stresses) are much more difficult to obtain. In principal, for the estimation of the thermal stress two things are required:

1. The inner wall temperature (T_i) and,
2. the temperature at the middle (average temperature) of the component (T_m).

Both values are not simple to determine. In the previous years there have been various different approaches to deal with this particular problem and some of them are described briefly in the following paragraphs.

Finite Element Analysis (FEA) is a very accurate method which can be used for the evaluation of structures and systems, providing a prediction to a component's response subjected to thermal and structural loads [10]. This method can model the three-dimensional shape of a component and can deal with different types of boundary conditions. The analysis is done by modeling the structure into a big number of small pieces (finite elements).

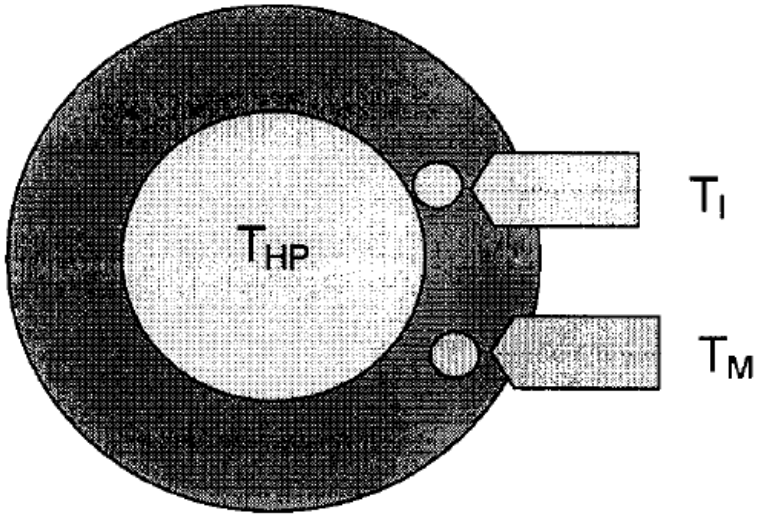

***Figure 1-3**: Cross-sectional view of thick-walled part with thermocouple inserts (Source: [6])*

The process of breaking the entire structure into such small pieces or elements is called discretization. The solution to the governing equations is closely approximated within each element, resulting in a number of equations that need to be solved for every element. However, each element interacts with its neighbors i.e. each element's response tightly depends on that of its neighbors and the responses of their neighbors to those of other neighbors, and so forth. Consequently, the element equations cannot be solved alone to render the solution over each element. Instead, all the equations from all the elements over the entire structure need to be solved simultaneously. Also, as the structure is broken into a larger number of elements, a greater number of simultaneous equations need to be solved. This requires high computing power which makes the FEA method slow and not suitable for an on-line monitoring system.

In many industrial applications thermal stresses are calculated from differential temperature measurements. For this purpose precision holes are drilled in the component for the inner and middle wall temperature measurements.

However this process has several disadvantages [6]:

- Measuring the differential temperature directly is costly (sensors, transducers, installation, commissioning, maintenance).
- The temperature of the thick-walled component is not calculated correctly. Due to the component loading, a gap of about 5 mm is left between the inner wall temperature measurement sensor tip and the inner surface. For this reason the measurement has a considerable delay in comparison to the actual inner wall temperature.
- Drilling weakens the material and is costly.
- Also the exact position of the sensors is difficult to obtain.

Another methodology that has been proposed and used successfully in the industry, is the use of mathematical models. These kind of models are capable of calculating the thermal stresses within critical components. The input variables of such models are the working fluid temperature and pressure and the output is an estimation of the evolution of stress.

In the past, Green's Function Technique (GFT) has been used to solve similar problems and it has been proven that the stress obtained is fairly coincided with that obtained by FEA [11]. As mentioned in Ref. [8], Riccardella et al. suggested a method based on GFT and Transfer Matrices. In this method, a simple linear transfer function is used to link two nodes in a finite element model. After the transfer function is produced, the response of one node to the other

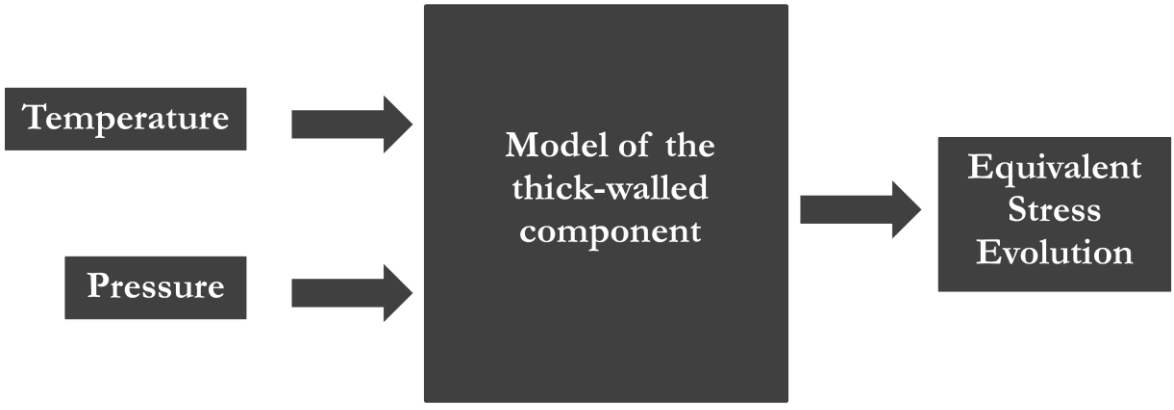

***Figure 1-4**: Mathematical model of a thick-walled component*

can be calculated if the latter is known. This method, however, only works in the forward direction. For most boiler applications the driving force for thermal stress is a change in the fluid temperature inside the component. When the outer surface temperature is known, it cannot be used to calculate the inner surface temperature.

Lu and Wilson [8], proposed a method based on Laplace transform through which the transfer functions between the fluid, inner and outer wall temperatures are derived. In this method the amount of on-line calculation is very small because the coefficients of the transfer functions can be pre-calculated off-line. Hence, this method could be suitable for a simulation model which uses on-line plant measurements to determine the evolution of stress.

Lausterer in [6], presents a method to calculate thermal stresses from readily available plant measurements. This method has been applied in a power plant resulting in decrease of instrumentation costs and improvement of the quality of the thermal stress calculation.

Similar mathematical models have been suggested by other authors [11, 12, 13] all of them concluding that the methods used are reasonably accurate, fast and suitable for use in stress monitoring and control systems.

1.4. Approach

The main purpose of the present study is to create a model that predicts the evolution of the thermomechanical stresses in a critical boiler component. In the following chart the logical approach that has been followed in this study is shown. Also, a brief description of each step is given.

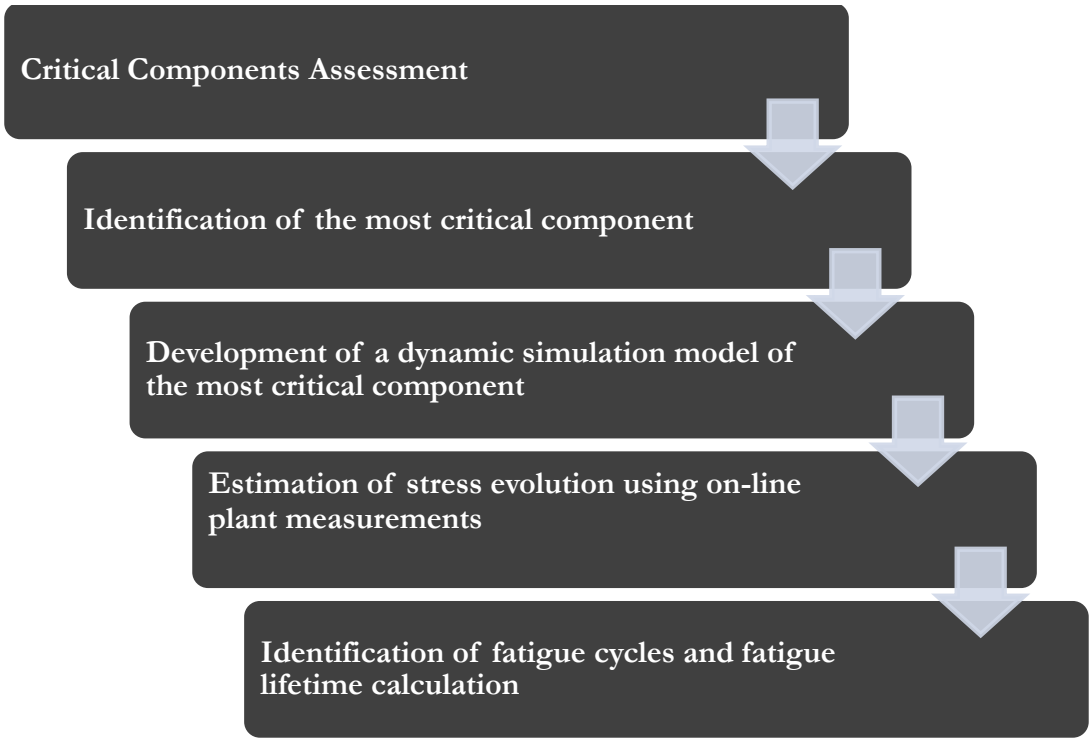

***Figure 1-5**: Approach of the study*

First, an assessment of the critical components is necessary. A HRSG has various components, however not all of them have the same criticality in terms of fatigue damage. Therefore, the European Norm EN 12952-3:2001 [14] is used to assess HRSG cumulative fatigue damage and to identify the most critical components of the HRSG. After identifying the most critical component, a more detailed investigation of the component is necessary.

Next, a model is developed in MATLAB-Simulink environment which predicts the evolution of stress in the most critical component. The inputs of this model is the transient signal of the steam conditions such as temperature and pressure and the output is the estimation of the equivalent stress evolution. This kind of model can be used in on-line monitoring and control applications for utility boilers such as HRSGs, fossil fuel boilers such as coal-fired boilers or biomass combustion boilers.

Then, by using the outputs of this model (equivalent stress evolution) a fatigue cycle counting method is applied in order to identify the fatigue cycles of the generated stress signal. This counting method is able of identifying fatigue cycles from random stress signals calculating their mean stress and stress amplitude.

Finally, based on the results of the fatigue cycle counting method, it is possible to make predictions for the existing plant in terms of fatigue lifetime by estimating the cumulative fatigue damage ratio.

2. MODERN FOSSIL FUEL BOILERS

In this chapter, a brief description of the main components that a modern boiler consists of is given. Then, the theory about the critical components of a boiler is discussed and a description of the method used to assess the critical components is presented.

2.1. Main Boiler Components

Modern steam generators or boilers, are a complex configuration of thermal-hydraulic (steam and water) sections which preheat and evaporate water, and superheat steam. These surfaces are arranged so that [15]:

1. the fuel can be burned completely and efficiently while minimizing emissions,
2. the steam is generated at the required flow rate, pressure and temperature and,
3. the maximum amount of energy is recovered.

The major components in a utility boiler include:

1. furnace and convection pass,
2. steam superheaters,
3. steam reheater,
4. economizer,
5. steam drum,
6. attemperator and steam temperature control system, and
7. air heater.

These components are supported by a number of subsystems and pieces of equipment such as combustion system, flues, ducts, fans and gas-side cleaning equipment.

In addition, another type of boiler is a Heat Recovery Steam Generator (HRSG). This kind of boiler has a similar configuration as a normal boiler with the difference that in a HRSG no fuel firing occurs since the exhaust gases from a gas turbine are used to produce steam.

In modern boilers, the furnace and convection pass walls are composed of steam- or water-cooled carbon steel or low alloy tubes. These tubes are connected at the top and bottom by headers, or manifolds. These headers distribute or collect the water, steam or steam-water mixture. The furnace wall tubes in most modern units also serve as key steam generating components or surfaces.

Superheaters and reheaters are specially designed in-line tube bundles that increase the temperature of saturated steam. In general terms, they are simple single-phase heat exchangers with steam flowing inside the tubes and the flue gas passing outside, generally in crossflow. These components are manufactured from steel alloy material because of their high operating

temperature. They are typically configured to help control steam outlet temperatures, keep metal temperatures within acceptable limits, and control steam flow pressure loss.

The main differences between superheaters and reheaters is the steam pressure. In a typical drum boiler the superheater outlet pressure might be 185 bar while the reheater outlet might be only 40 bar. The superheater and sometimes reheater are often divided into multiple sections to help control steam temperature and optimize heat recovery.

The economizer is a counterflow heat exchanger for recovering energy from the flue gas. It increases the temperature of the water entering the steam drum. The tube bundle is typically an arrangement of parallel horizontal serpentine tubes with the water flowing inside but in the opposite direction (counterflow) to the gas. Tube spacing is as tight as possible to promote heat transfer while still permitting adequate tube surface cleaning and limiting flue gas-side pressure loss. By design, steam is usually not generated inside these tubes.

The steam drum is a large cylindrical vessel at the top of the boiler in which saturated steam is separated from the steam-water mixture leaving the boiler tubes. Drums can be quite large with diameters of 0.9 to 2 m and lengths in the order of 30 m. They are fabricated from thick steel plates rolled into cylinders with hemispherical heads. They house the steam-water separation equipment, purify the steam, mix the replacement or feedwater and chemicals, and provide limited water storage to accommodate small changes in unit load. Major connections to the steam drum are provided to receive the steam-water mixture from the boiler tubes, remove saturated steam, add replacement or makeup water, and return the near saturated water back to the inlet of the boiler tubes.

The steam temperature control system can be complex and includes combinations of recirculating some of the flue gas to the bottom or top of the furnace, providing special gas flow passages at the back end of the steam generator, adjusting the combustion system, and adding water or low temperature steam to the high temperature steam flow (attemperation). The component most frequently used for the latter is called spray attemperator. In large utility units, attemperators with direct injection of water or low temperature steam are used for dynamic control because of their rapid response. They are specially designed to resist thermal shock and are frequently located at the inlet of the superheater or between superheater sections to better control the superheater outlet metal temperatures. Positioning of individual superheater sections can also help maintain proper outlet steam temperatures.

The air heater is not a part of the steam-water circuit, but plays an important role in the steam generator system heat transfer and efficiency. In many cases, especially in high pressure boilers, the temperature of the flue gas leaving the economizer is still quite high. The air heater recovers much of this energy and adds it to the combustion air to reduce fuel use. Designs include tubular, flat plate, and regenerative heat exchangers, among others.

2.2. Critical Boiler Components

As mentioned in the previous chapter, a boiler has various components. However some of them are more likely to get fatigue damage faster than others. More specifically, in cylindrical

vessels the temperature distribution is dependent only upon the ratio of the outer and inner radii, and normally, greater total temperature differences are associated with increased thickness. Hence, thick-walled vessels are more susceptible to failure due to thermal stresses than are thin ones [16]. For example, according to Decoussemaeker et al. [9], thick-walled components such as steam drums or superheater outlet headers can develop significant through-wall temperature gradients during start-up. Also, large temperature differences can occur at junctions between thick- and thin-walled parts, such as tube-to-header connections. These components are the so-called critical components, which need further investigation. If these relatively thick-walled components subjected to the highest temperatures and rates of temperature change meet the cycling requirements then, theoretically, the other components of the boiler will also meet the cycling requirements because other parts are of lesser wall thickness and subject to less significant transients.

The first step of the present study is to determine which the critical components are. This is possible by using the relevant sections of the European Standard EN 12952-3:2001 [14]. The purpose of this code is to calculate the fatigue damage factor of a component under cyclic operation.

The component with the higher fatigue damage factor is considered as the most critical one and it will be studied in more detail. Also, it is expected that the critical components obtained by the use of the European Norm to be in agreement with the literature references.

2.3. Methodology for Critical Components Assessment

In this section the methodology used in order to identify the critical components of a boiler is briefly described. The method is in accordance with the relevant sections of the European Standard EN 12952-3:2001 and EN 12952-4:2000 [14]. As already mentioned, the purpose of this code is to calculate the cumulative fatigue damage factor or cycle damage ratio of a component under cyclic operation. A detailed description of the assumptions and the formulation of the code is given in Appendix A.

The main inputs of the EN 12952-3 code are the process data in terms of minimum and maximum pressure and temperature. Also, the component dimensions have to be specified. Moreover, the component's material properties are an important input too. Finally, the rate of temperature change must be specified. The temperature change varies for different components and under different cycles (hot/cold start, start-up/shut down etc.). A high temperature change means that the plant has a very quick response in load changes, making it flexible, nevertheless this has a big influence in the lifetime of the components in the boiler. Hence, the rate of temperature change is a determining factor for computing the damage factor of different components.

The cumulative fatigue damage factor is calculated using Miner's rule. Miner's rule is one of the most widely used cumulative damage models for failure caused by fatigue. It is called 'Miner's rule' because it was popularized by M. A. Miner in 1945 [17].

Miner's rule is probably the simplest cumulative damage model. It states that if there are k different stress levels and the average number of cycles to failure at the i_{th} stress, σ_i, is N_i, then the damage ratio, C, is:

$$C = \sum_{i=1}^{k} \frac{n_i}{N_i} \ , \tag{2-1}$$

Where n is the number of cycles at stress σ and N is the number of cycles to failure at same stress σ. N could be determined from σ-N curves for the material.

The damage factor represents the fraction of the total life which is expended by the cycles that occur at a particular stress value. A damage factor less than unity indicates that the component is likely to endure the required cyclic service without risk of cracking.

After the implementation of the EN 12952-3 to various thick-walled components, the component with the higher cumulative fatigue damage factor (under the same cyclic conditions) is considered as the most critical.

3. DYNAMIC MODEL DEVELOPMENT

In this chapter, a model is developed in MATLAB-Simulink environment in order to calculate the evolution of the thermomechanical stresses in a critical boiler component. All the mathematical formulation is given along with the assumptions that have been made. In addition, a method for counting the fatigue cycles in a random stress signal is described and finally the estimation of the fatigue damage ratio is discussed.

3.1. Modeling Assumptions

A very important aspect of the modeling process is the formulation that has been used for calculating the heat transfer phenomena and eventually the actual stresses that are developed. This is based on a number of assumptions which are usually necessary in order to make the problem simpler and easier for the application. A summary is given below of the assumptions applied in this work.

- The component is a long hollow cylinder. Usually that is the case for boiler components. Steam drums, superheater headers/manifolds etc. are components with a cylindrical geometry and large length compared to their radius.
- The temperature at the inner surface is spatially constant in the axial as well tangential direction. Hence, the temperature T(r,t) within the component depends only on radius r and time t. According to Ref. [18], this is generally true when the component is completely heated up. However, in a cold start-up process, the temperature might differ at different points in the tangential as well as axial direction (see Figure 3-1).

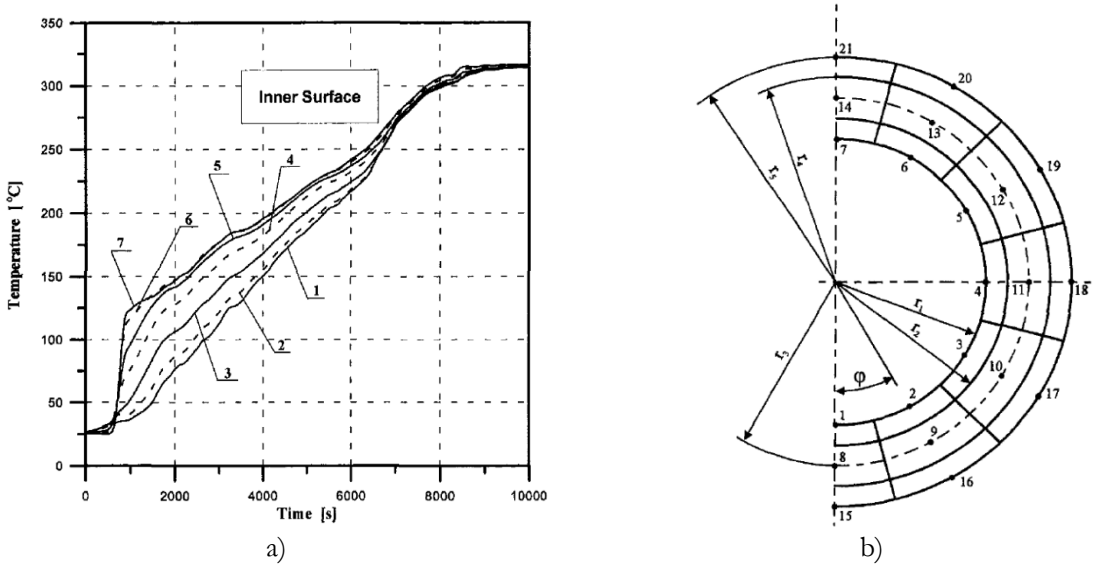

***Figure 3-1**: a) Temperature changes at different points on inner surface of a drum during a cold start-up, b) Half cross section of the steam drum where the different points 1-7 are shown (Source: [18])*

- The component is perfectly thermally insulated. This means that the heat loss through the insulated wall is negligibly small compared to the heat transfer to the component. That is true only in the case of a drum which has a thick insulating layer.
- The material properties are based on the reference temperature t* as it is defined in Appendix A. In principal, the material properties change with temperature. However, this is very difficult to be included in the simulation calculations. Therefore, a reference temperature is defined (as in [14]) and the material properties at this temperature are used. Fortunately, this could be a good approximation since, the material properties are not changing significantly with the temperature (acc. to material properties tables in [14]).
- The temperature gradient across the component's wall thickness is linear. In relation to the material properties assumption, a constant value is used for the thermal conductivity of the metal. That also requires the assumption that even though the component has an annular geometry, due to its large mean diameter, the geometry can be eventually considered as a flat plate.

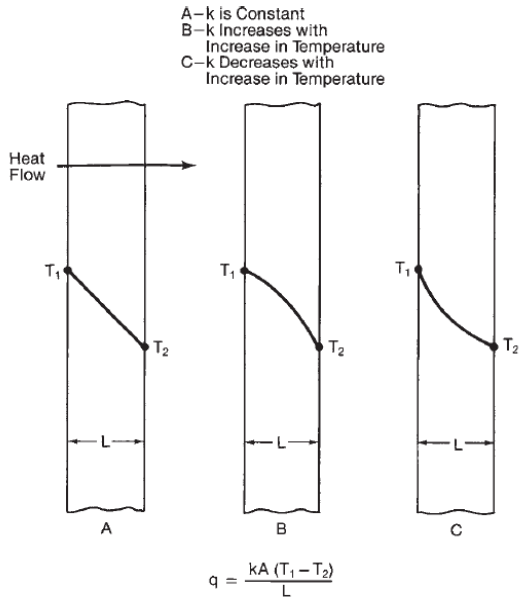

***Figure 3-2**: Temperature-thickness relationships corresponding to different thermal conductivities, k (Source: [15])*

3.2. Estimation of Stress Evolution

As already mentioned, the fatigue damage in a component is a function of stresses due to thermal transient (thermal stresses) and to pressure (mechanical stresses). In the following chapters a detailed description is given of how the mechanical and thermal stresses can be calculated and introduced to a simulation model.

Mechanical stresses

The calculation of the mechanical stresses due to pressure can be calculated using Lame's solution [16]:

$$\sigma_r = \frac{r_i^2 p_i - r_o^2 p_o}{r_o^2 - r_i^2} - \frac{(p_i - p_o) r_i^2 r_o^2}{r^2 (r_o^2 - r_i^2)} \tag{3-1}$$

$$\sigma_t = \frac{r_i^2 p_i - r_o^2 p_o}{r_o^2 - r_i^2} + \frac{(p_i - p_o) r_i^2 r_o^2}{r^2 (r_o^2 - r_i^2)} \tag{3-2}$$

$$\sigma_z = \frac{(p_i - p_o) r_i^2 r_o^2}{r^2 (r_o^2 - r_i^2)} \tag{3-3}$$

$$r_i < r < r_o$$

After inspection of the above equations, it can be seen that the maximum tangential and axial stresses occur at the inner side of the cylinder. Also, the maximum radial stress is the larger of p_i and p_o and it occurs at the inner side of the cylinder as well. Hence, considering the worst case scenario, it is safe to focus at the distribution of the mechanical stresses only at the inner side. Moreover, by assuming that the component is under internal pressure only (p_o=0), the above equations are reduced to:

$$\sigma_r = \frac{r_i^2 p_i}{r_o^2 - r_i^2} \left(1 - \frac{r_o^2}{r_i^2} \right) = -p_i \tag{3-4}$$

$$\sigma_t = \frac{p_i (r_i^2 + r_o^2)}{r_o^2 - r_i^2} \tag{3-5}$$

$$\sigma_z = \frac{p_i r_o^2}{r_o^2 - r_i^2} \tag{3-6}$$

Thermal stresses

As already discussed, the stresses due to thermal transients are more difficult to estimate. In general, thermal stresses occur when there is a temperature difference across the wall of a component. In boiler components, the wall temperature transients are usually caused by changes in temperature of the fluid inside the pipe. In practice, the thermal stresses are calculated using invasive metal temperature measurements. However, the inner surface temperature is difficult to measure since internal transducers require cable seals which can compromise the integrity of the pressure wall, and the possible detachment of these transducers may cause damage to some other part of the plant. Also, measuring the differential temperature directly becomes costly in terms of sensors, transducers, installation, commissioning and maintenance [6]. Therefore, the practical solution is to measure the temperature on the outer surface of the component and by using mathematical models the inner wall temperature can be predicted and as a result the thermal stresses.

For this investigation, the method suggested by Lu and Wilson [8] is used. This method is based on Laplace transform through which the transfer functions between the fluid, inner and outer wall temperatures are derived.

The principal thermal stresses can be calculated from the following expressions [19]:

$$\sigma_r = \frac{aE}{(1-\nu)r^2}\left[\frac{r^2-r_i^2}{r_o^2-r_i^2}\int_{r_i}^{r_o} Tr\,dr - \int_{r_i}^{r} Tr\,dr\right] \tag{3-7}$$

$$\sigma_t = \frac{aE}{(1-\nu)r^2}\left[\frac{r^2+r_i^2}{r_o^2-r_i^2}\int_{r_i}^{r_o} Tr\,dr + \int_{r_i}^{r} Tr\,dr - Tr^2\right] \tag{3-8}$$

$$\sigma_z = \frac{aE}{(1-\nu)}\left[\frac{2}{r_o^2-r_i^2}\int_{r_i}^{r_o} Tr\,dr - T\right] \tag{3-9}$$

As in the case of mechanical stresses, the maximum thermal stresses in the tangential and axial direction occur at the inner part of the cylinder, whereas the radial stresses are maximum at the centre of the wall thickness and become zero at the inner and outer surface. Moreover, this has been proven from previous studies [6, 11, 20, 21, 22, 23] hence in this model only the inner thermal stresses are calculated.

It is common that the thermal gradient throughout the cylindrical vessel wall cannot be simply expressed, hence an analytical solution of the above equations is not readily obtainable. However, the tangential stress may be written as:

$$\sigma_t = \frac{aE}{(1-\nu)}\left[\frac{r^2+r_i^2}{r^2(r_o^2-r_i^2)}\int_{r_i}^{r_o} Tr\,dr + \frac{1}{r^2}\int_{r_i}^{r} Tr\,dr - T\right] \tag{3-10}$$

The first integral can be expressed as (under the assumption that $r = r_i$):

$$\frac{1+\frac{r_i^2}{r^2}}{r_o^2-r_i^2}\int_{r_i}^{r_o} Tr\,dr = \frac{\int_{r_i}^{r_o} 2\pi Tr\,dr}{\pi(r_o^2-r_i^2)} \tag{3-11}$$

which represents the mean value of the temperature throughout the entire wall thickness. In addition, for $r = r_i$ the second integral becomes zero. Thus, the tangential stress at the inner surface can be written as:

$$\sigma_t = \frac{aE}{1-\nu}[\mathrm{T_m} - \mathrm{T_i}]\ , \tag{3-12}$$

Where T_m is the mean temperature of the entire cylindrical wall thickness and T_i the temperature at the inner surface.

Furthermore, according to equation 3-9, the axial stress is expressed as:

$$\sigma_z = \frac{aE}{(1-\nu)}\left[\frac{2}{r_o^2 - r_i^2}\int_{r_i}^{r_o} Tr\,dr - T\right] \tag{3-13}$$

and the integral may be written as:

$$\frac{2}{r_o^2 - r_i^2}\int_{r_i}^{r_o} Tr\,dr = \frac{\int_{r_i}^{r_o} 2Tr\,dr}{r_o^2 - r_i^2} = \frac{\int_{r_i}^{r_o} 2\pi Tr\,dr}{\pi(r_o^2 - r_i^2)} \tag{3-14}$$

which again is the mean value of the temperature throughout the wall thickness. Hence, the axial stress can be expressed with the same formula as in the situation of the tangential stress.

Considering that the radial stress is zero at the inner surface, the general equation that can be used for the calculation of the thermal stresses in the tangential or axial direction is:

$$\sigma = \frac{aE}{1-\nu}[\mathrm{T_m} - \mathrm{T_i}] \tag{3-15}$$

As mentioned before, the two parameters necessary for the calculation of the thermal stresses are the average temperature across the wall thickness (T_m) and the metal temperature at the inner surface (T_i). Since a linear temperature gradient across the wall of the component is assumed, the mean temperature can be calculated as:

$$T_m = \frac{T_i + T_o}{2}\ , \tag{3-16}$$

Where T_o is the outer surface (skin) temperature which can be easily derived from the plant measurements.

Finally, the mean temperature and stress can be calculated when T_i is known, hence the following method focuses on calculating T_i.

Estimation of the inner surface temperature

According to Lu and Wilson [8], when the fluid temperature is known, the transfer function between the inner surface temperature of the cylindrical vessel and the fluid temperature is:

$$G_f(1,s) = \frac{\bar{T}(1,s)}{\bar{T}_f} = \frac{\sum_{i=0}^{\infty}\frac{1}{(2i)!}s^i}{\sum_{i=0}^{\infty}\frac{2i/_B + 1}{(2i)!}s^i} \tag{3-17}$$

$$B = \frac{hL}{k}\ , \tag{3-18}$$

Where $\bar{T}_f$ is the saturated fluid temperature (dimensionless) and $\bar{T}(1,s)$ the inner surface temperature (dimensionless).

It is important to mention that during the simulation dimensionless time and temperature is used by introducing the following:

$$\bar{T}_f(t) = \frac{T_f(t) - T_0}{T_0} \tag{3-19}$$

$$\bar{t} = \frac{t}{L^2/D_{th}} \ , \tag{3-20}$$

Where T_0 is the initial temperature and D_{th} the thermal diffusivity.

Moreover, after estimating the inner temperature, it is possible to estimate the outer temperature by using the following transfer function:

$$G_o(1,s) = \frac{\bar{T}(1,s)}{\bar{T}(0,s)} = \sum_{i=0}^{\infty} \frac{1}{(2i)!} s^i \implies \bar{T}(0,s) = \bar{T}(1,s) \sum_{i=0}^{\infty} \frac{(2i)!}{s^i} \tag{3-21}$$

The outer temperature can be then compared with real plant measurements in order to estimate the proper heat transfer coefficient inside the component. This is useful especially in the case of a steam drum where the fluid is a mixture of steam and water which makes the determination of the heat transfer coefficient difficult.

After estimating the inner and outer temperatures based on the fluid temperature, an estimation of the thermal stresses is possible.

Equivalent stress calculation

By estimating the mechanical and thermal stresses, the three principal structural stresses in the metal of the steam drum are calculated by applying the superposition principal to thermal (σ^T) and mechanical (σ^P) stresses as follows:

$$\sigma_t = \sigma_t^P + \sigma_t^T \tag{3-22}$$

$$\sigma_r = \sigma_r^P + \sigma_r^T \tag{3-23}$$

$$\sigma_z = \sigma_z^P + \sigma_z^T \tag{3-24}$$

Then, the equivalent stress can be calculated. There are two main criteria suggested by Von Mises and Tresca. The main expressions are the following [24]:

$$\sigma_{eq,Von\ Mises} = [\sigma_t^2 + \sigma_r^2 + \sigma_z^2 - (\sigma_t\sigma_r + \sigma_r\sigma_z + \sigma_z\sigma_t)]^{1/2} \tag{3-25}$$

$$\sigma_{eq,Tresca} = max(|\sigma_t - \sigma_r|, |\sigma_r - \sigma_z|, |\sigma_z - \sigma_t|) \quad (3\text{-}26)$$

Validation of the model's performance

By implementing the aforementioned equations, a model is developed in MATLAB-Simulink environment (see Appendix C).

In order to validate the performance of the model, a superheater header is simulated as in Ref. [8]. The thickness of the header is L=80 mm, the heat conductivity of the metal is k=31 W/mK and the heat transfer coefficient between the fluid and the metal is h=800 W/m^{2}K. Simulations have been done for a step change in the fluid temperature.

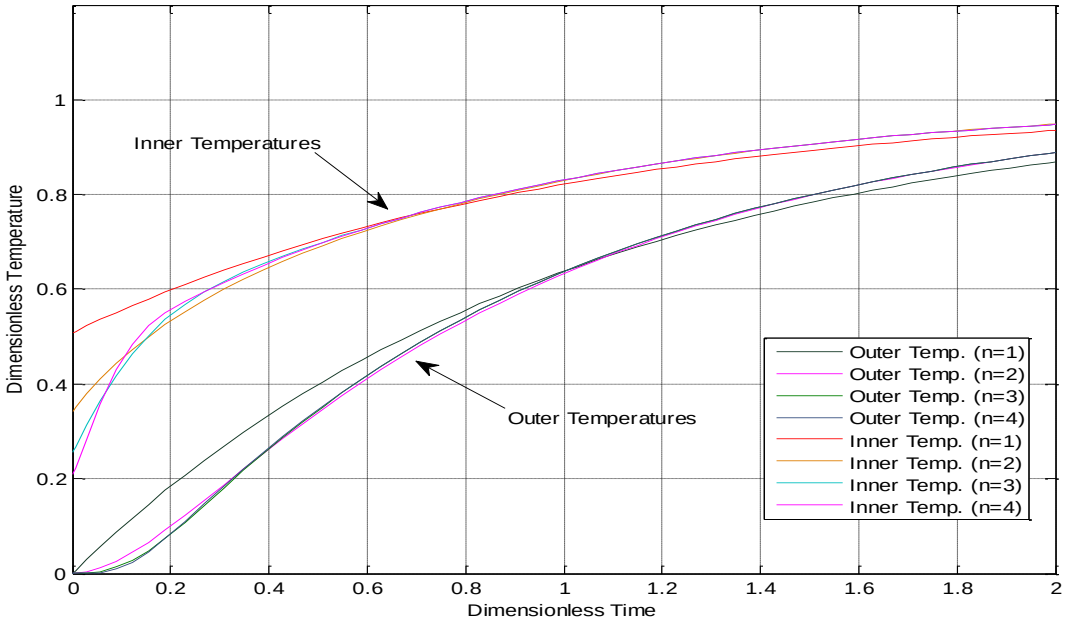

***Figure 3-3**: Responses of header temperatures to step change on fluid temperature*

Figure 3-3 shows the inner and outer surface temperature responses of the header to a step change in fluid temperature. n=1, 2, 3 and 4 mean that the transfer function consists of up to 1st, 2nd, 3rd and 4th-order of operator s, respectively. It can be seen that the accuracy of the transfer function increases with n. According to Ref. [8] (also visible from Figure 3-3) a 3rd-order transfer function may be accurate enough for engineering applications.

In addition, as shown in Figure 3-4, the accurate solution matches very well with a 3rd-order transfer function. Hence, for the simulation calculations a 3rd-order transfer function will be used.

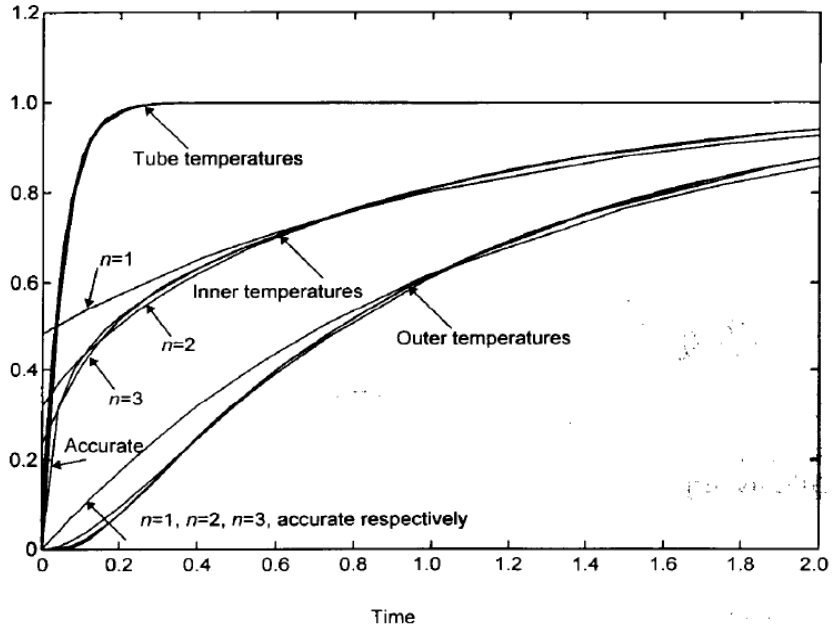

***Figure 3-4**: Responses of tube and header temperatures to step change in fluid temperature as reported in Ref.[8]*

3.3. The Identification of Fatigue Cycles

After estimating the equivalent stress using either the Tresca or Von Mises criteria, it is possible to determine the fatigue cycles for a specific load time history. There are several methods for counting fatigue cycles. However, in the present study the "rainflow counting method" has been used since, as suggested by other authors in [13] and [25], it is one of the most popular and widely used algorithms. Also according to [11], rainflow cycle counting algorithm has proved to be superior to other cycle counting methods for analyzing irregular stress. According to Socie [26], the apparent reason for the superiority of the rainflow cycle counting algorithm is that it combines load reversals in a manner that defines a cycle as a closed hysteresis loop. Each closed hysteresis loop has a strain range and mean stress associated with it that can be compared with the constant amplitude fatigue data in order to compute the fatigue usage factor. In this method, the cycle is counted such that small stress excursions are considered as temporary interruptions of larger stress excursions. It matches the highest peak and deepest valley, in descending order, until all peaks and valleys are paired. From the stress cycles, the fatigue usage factor is computed using the material fatigue curve. In the present study, the guidelines reported in [25] have been followed.

With the rainflow algorithm it is possible to assign amplitudes and mean values of distinguished cycles from random loading history. The importance of the algorithm is that it allows the application of Miner's rule in order to assess the fatigue life of a structure subject to complex loading. The main input to such an algorithm is the signed Tresca or Von Mises equivalent stress as a function of time. Then the signal is treated to individuate "peaks" and "valleys" or, as also mentioned, "turning points". As noted in ASTM E 1049 Standard [27], a "peak" in fatigue loading is the point at which the first derivative of the load time history changes from a

positive to a negative sign. Respectively, in the case of a "valley" the opposite occurs. The main outputs of the algorithm, for each identified cycle are:

- The peak amplitude $\Delta\sigma/2$
- The mean value (algebraic average of the peak and valley values) σ_m
- The value 0.5 if the stress range is counted as a half-cycle or the value 1 if it is counted as one cycle
- The cycle beginning time t_0
- The cycle period τ

Working principle

According to the SAE and ASTM standards [27, 28], the rainflow cycle counting rule uses three consecutive points in a load time history to determine whether a cycle is formed. Figure 3-5 shows the rules that identify the two possible closed cycles in a time history where stress is the load parameter. The three consecutive stress points (S_1, S_2, S_3) define the two consecutive ranges as $\Delta S_1 = |S_1 - S_2|$ and $\Delta S_2 = |S_2 - S_3|$. If $\Delta S_1 \leq \Delta S_2$, one cycle from S_1 to S_2 is extracted, and if $\Delta S_1 > \Delta S_2$, no cycle is counted. The method requires that the stress time history be arranged so that it contains only the peaks and valleys and it starts with either the highest peak or the lowest valley, whichever is greater in absolute value. Then, the cycle identification rule is applied to check every three consecutive points from the beginning until a closed loop is defined. The two points forming the cycle are discarded and the remaining points are connected to each other. This procedure is repeated from the beginning until the remaining data are exhausted [28].

Nevertheless, for the present study a variation of the rainflow algorithm is used as suggested by Downing and Socie [29]. This variation applies the same rule for a cycle extraction to a load time history and does not require the load sequence to start with either the maximum peak or the minimum valley.

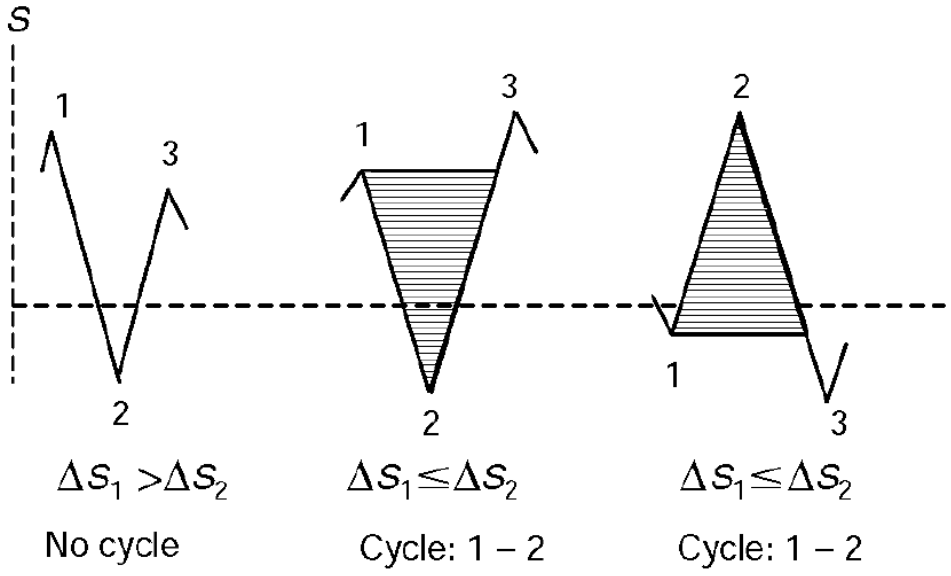

***Figure 3-5**: Rules of rainflow cycle counting [28]*

Example

As an example, the signal depicted in Figure 3-6 is used as an input to the algorithm. By using the rainflow algorithm developed in the MATLAB environment [30] (see Appendix C), it is possible to count the cycles according to rainflow algorithm, and to state the time of the cycle occurrence and the cycle periods. The extracted cycles are depicted in Figure 3-7. The obtained values are presented in Table 3-1.

From the results it can be seen that the algorithm calculates 3 cycles and 4 half-cycles. Thus in total, 5 fatigue cycles are counted.

***Table 3-1**: Values readout and computed for the counted cycles*

Number of the cycle or half-cycle	C1	C2	C3	C4	C5	C6	C7
Amplitude $\Delta\sigma/2$ (MPa)	1	3	1.5	0.5	5	2.5	1
Mean value σ_m (MPa)	-1	-2	-0.5	2.5	0	2.5	1
Cycle or half-cycle	1	0.5	1	1	0.5	0.5	0.5
Cycle beginning time t_0 (s)	1	0	5.5	7.5	4	8.5	9.5
Period τ (s)	2	8	2	1	9	2	1

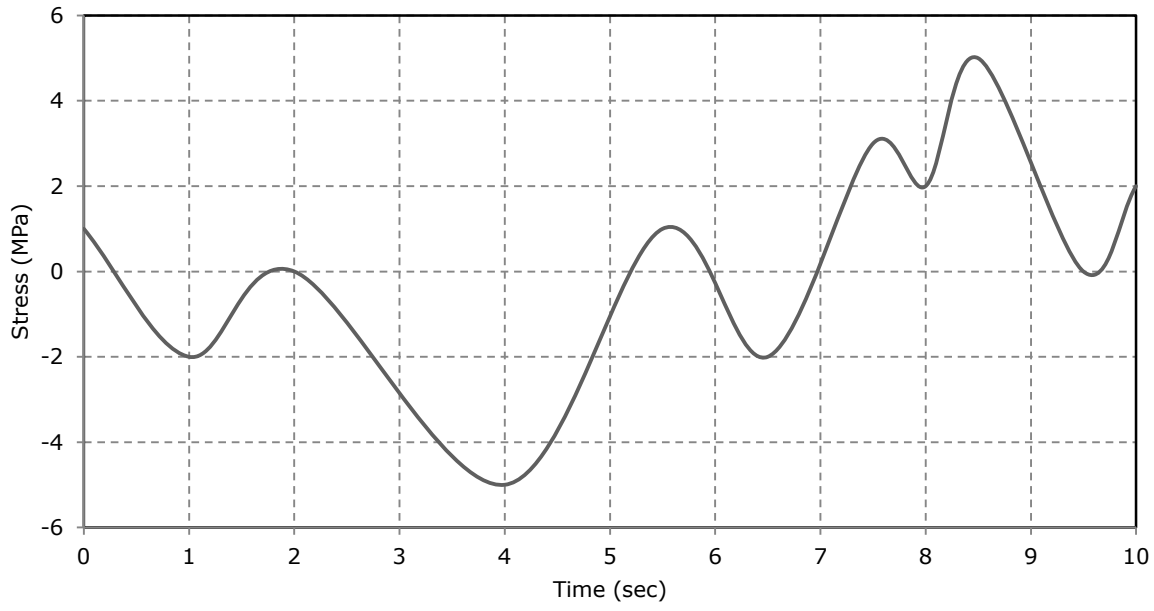

***Figure 3-6**: Load time history of a stress signal*

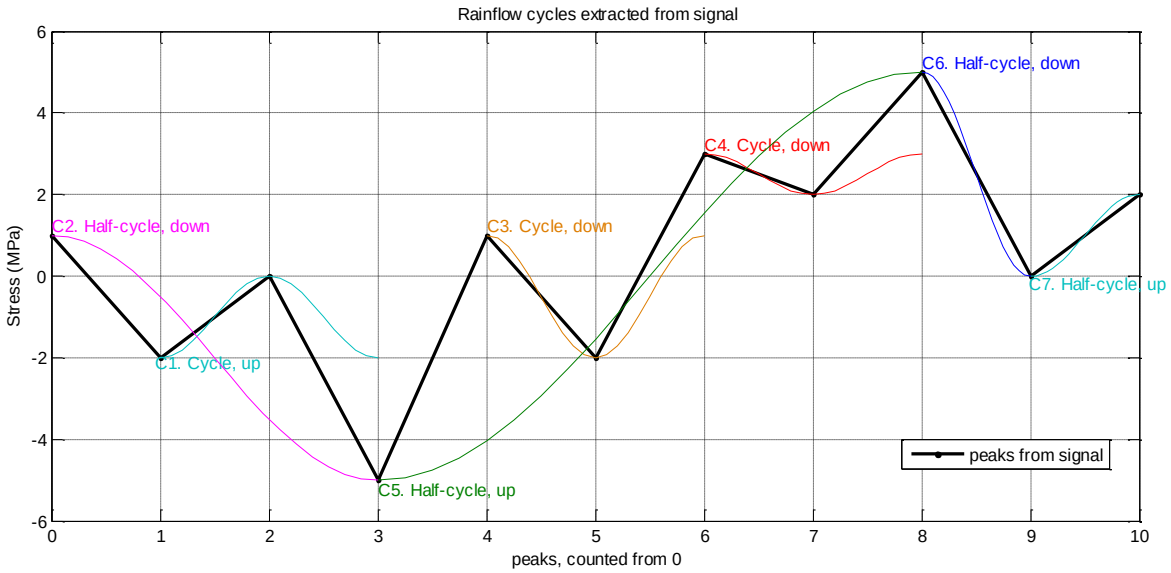

***Figure 3-7**: Turning points with cycles and half-cycles counted using the rainflow algorithm*

The following histograms depict the amplitude and the mean value of the fatigue cycles identified by the rainflow algorithm.

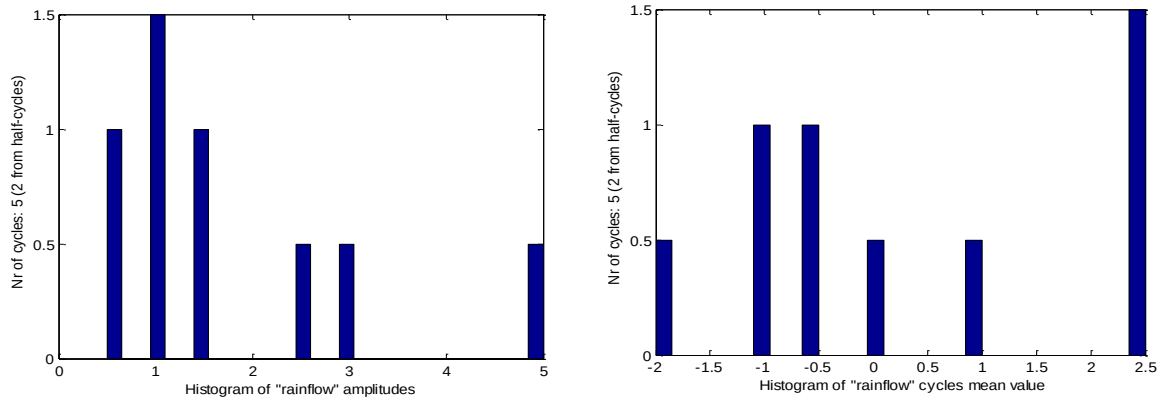

***Figure 3-8:** Histograms of amplitude and mean value of fatigue cycles*

3.4. Fatigue Lifetime Prediction

When the fatigue cycles are identified, it is possible to determine a cumulative fatigue damage ratio. The methodology used for the determination of the fatigue damage ratio depends on the type of fatigue that occurs. In practice, a component is exposed to a complex, often random, sequence of loads. This can lead to a high-cycle or a low-cycle fatigue.

In high-cycle fatigue the stresses are well below the yield strength, hence there is a high number of load cycles to failure (i.e. the fatigue lifetime). On the other hand, in low-cycle fatigue there is plastic deformation in each fatigue cycle thus a low number of cycles to failure exists.

In a high-cycle fatigue situation, the performance of the material can be characterized by an S-N curve, also known as Wöhler curve.

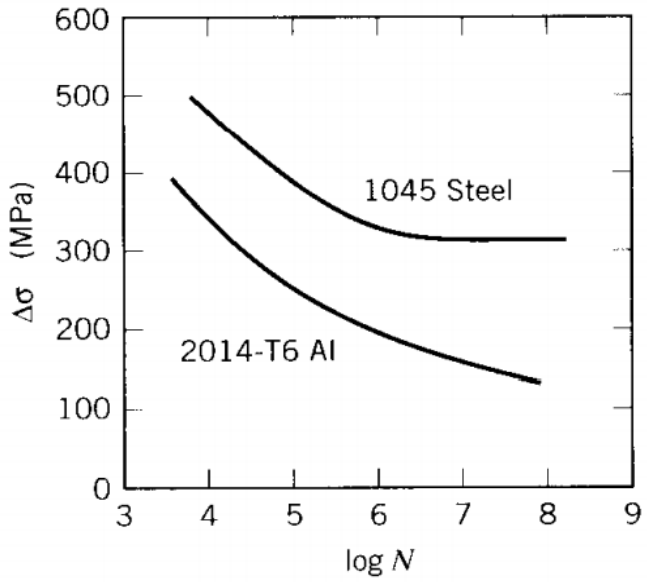

***Figure 3-9**: S-N curves for aluminum and low-carbon steel (Source: [31])*

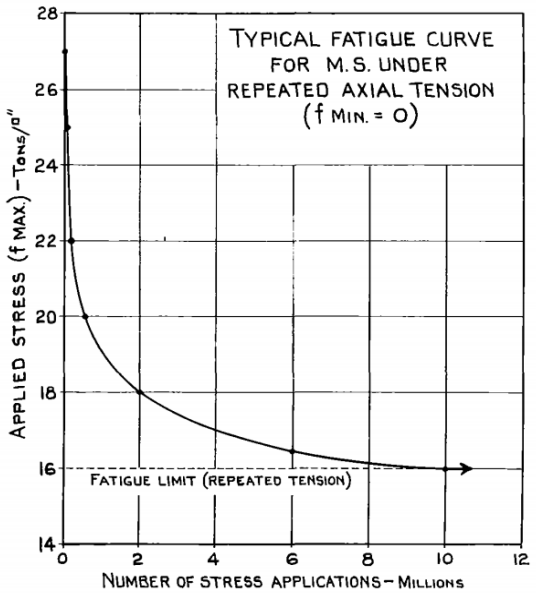

***Figure 3-10**: Typical S-N curve for low carbon steel under axial tension (Source: [32])*

In this kind of diagrams, a constant cyclic stress amplitude S is applied to a specimen and the number of loading cycles N until the specimen fails is determined. Millions of cycles might be required to cause failure at lower loading levels, so the abscissa is usually plotted logarithmically. In some materials, such as ferrous alloys, the S-N curve flattens out eventually, so that below a certain endurance limit failure does not occur no matter how long the loads are cycled. However, as some studies suggest [33], in reality even small stress amplitudes can cause fatigue failure eventually.

In a low-cycle fatigue situation, the material is usually characterized by the Coffin-Manson relation:

$$\frac{\Delta\varepsilon_p}{2} = \varepsilon_f'(2N_f)^c \tag{3-27}$$

Where,

$\Delta\varepsilon_p/2$ is the plastic strain amplitude,

ε_f' is an empirical constant known as the fatigue ductility coefficient (i.e. the failure strain for a single reversal),

$2N_f$ are the number of load reversals to failure,

c is an empirical constant known as fatigue ductility exponent.

In low-cycle fatigue using the stress amplitude, $\Delta\sigma/2$, as the ruling mechanical parameter would not be appropriate since a small change in $\Delta\sigma/2$ would already give a significant change in $\Delta\varepsilon/2$. Moreover, plasticity is the reason underlying the fatigue phenomenon.

Depending on the situation (high-cycle or low-cycle fatigue) the allowable cycles till failure can be determined and then the cumulative fatigue damage can be estimated using Miner's rule as mentioned in Chapter 2.3.

4. CASE STUDY

After implementing and validating the performance of the model, it is possible to apply it in a real power plant using on-line plant measurements. In this study the HRSG of the Maxima Power Plant, a Gas Turbine Combined Cycle (GTCC) power plant, is simulated. First a brief description of the plant is given and then an assessment of the most critical components is performed. Depending on the results of the assessment, the simulation model is applied on the most critical component. Moreover, the simulation is held for different transient operation modes. These include:

1. Load change
2. Typical 24h operation
3. Shut down
4. Start-up

Load Change

Load change means ramping from a certain steady power output, for instance 60% part-load, to a different power output. This can be higher or lower than 60% part-load. During normal operation the power output is almost never constant. It changes due to the electricity price on the market and consumer demand. Hence, fatigue cycles are expected to occur.

Typical 24h Operation

An interesting simulation is a 24h daily operation of a modern GTCC. By simulating a daily operation, valuable conclusions can be drawn concerning the cycling operation of the plant.

Shut down

Shut down of the plant could happen in two different ways: planned shut down of the plant or a trip. In a planned shut down the cooling down of the Gas Turbine (GT) and HRSG is controlled. In a situation where a trip occurs, the GT is shut down immediately and is thus more likely to impose large thermal transients on the HRSG due to the rapid cooling.

Start-up

A start-up is a delicate procedure because GT load can be increased faster than the HRSG. This leads to a fast increase of temperature and mass flow rate at the flue gas side. The cold start-up time of typical HRSGs ranges from 45 minutes to 2 hours or more. The most critical fact during start-up is the rapid increase of all operating parameters including temperature, pressure and mass flow. During that period, HRSG components, especially the steam drum, are subject to high thermal stress, which is generated by the uneven distribution of the metal temperature [21].

4.1. Maxima Power Plant

The Maxima power plant is a GTCC plant located close to the city of Lelystad in the province of Flevoland in the Netherlands. It consists of two identical single shaft KA-26 units. It uses natural gas as main fuel and has a total power output of 880 MWe.

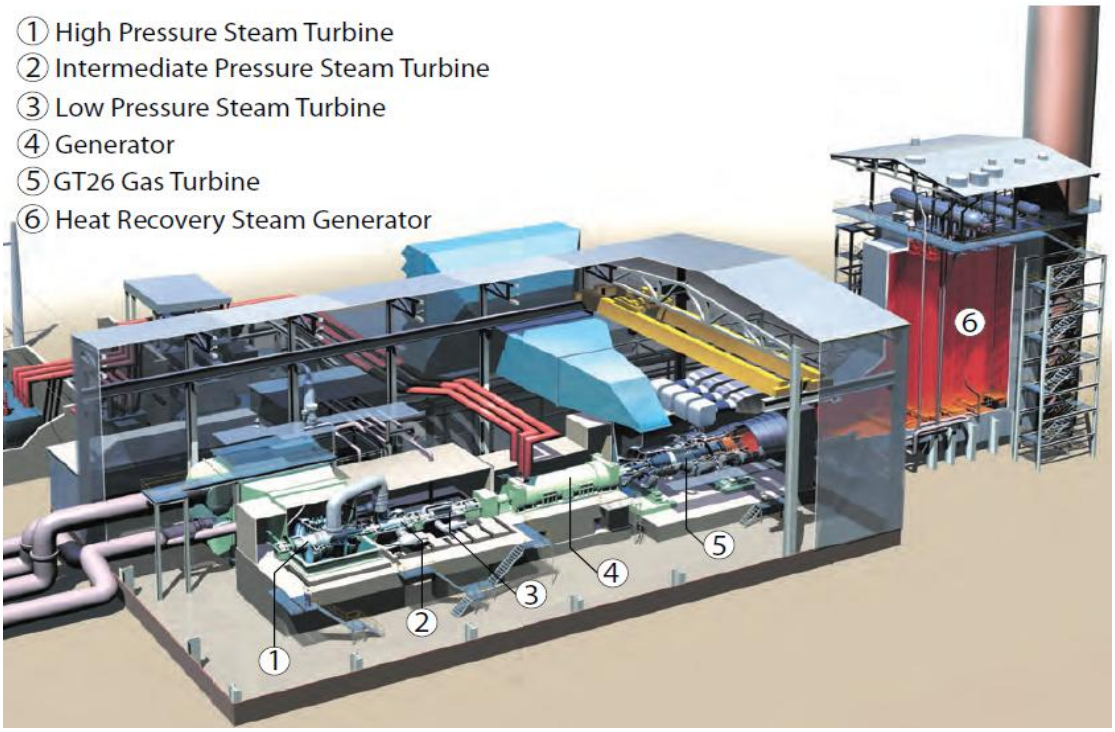

***Figure 4-1**: Schematic overview of KA-26 unit*

Single shaft means that the three parts of the steam turbine i.e. the high pressure, intermediate pressure and low pressure (1, 2, 3 in Figure 4-1) and the gas turbine (5 in Figure 4-1) are connected to the same shaft driving the generator (4 in Figure 4-1). The main component of the KA-26 power plant is the GT26 gas turbine, a two stage combustion design, first introduced in 1990.

The exhaust gases from the gas turbine are lead into the HRSG (6 in Figure 4-1), the produced steam drives the steam turbines producing a total of 160 MWe.

Heat Recovery Steam Generator

Figure 4-2 is a schematic overview of the Maxima Power Plant. At the upper part of the graph the HRSG is depicted and the various components that it consists of are visible. More specifically this HRSG is fitted with three steam drums each operating at a different pressure level indicated by Low Pressure (LP), Intermediate Pressure (IP) and High Pressure (HP).

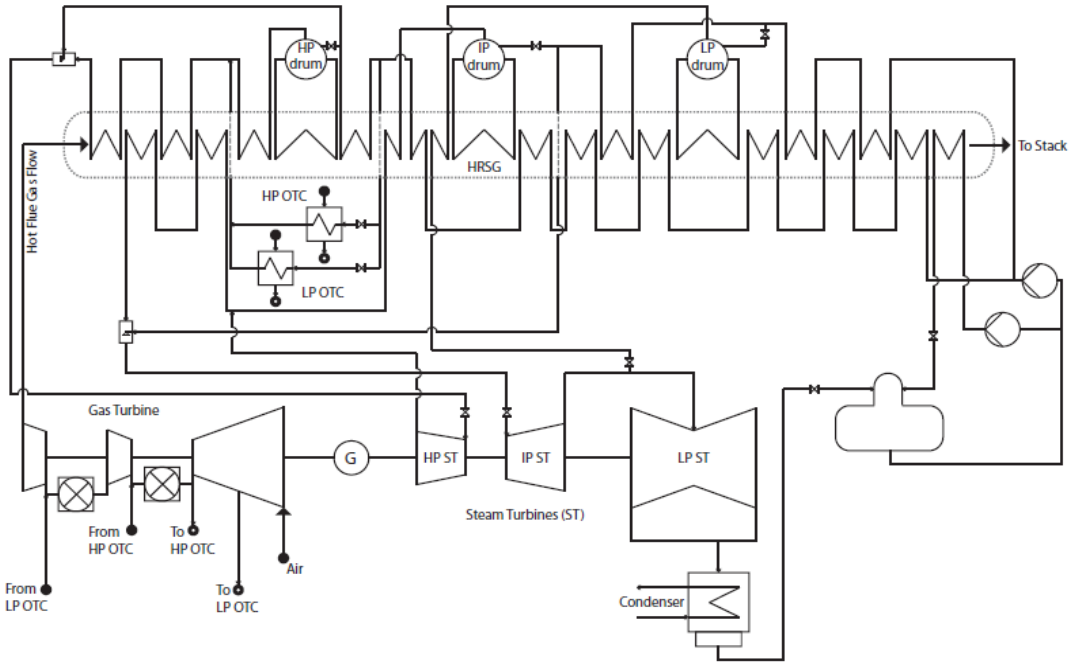

***Figure 4-2**: Schematic overview of the Maxima Power Plant*

The high pressure steam is led into the HP steam turbine. Once the steam is expanded over the turbine it is sent back to the HRSG. There it joins the IP steam in the reheaters which is sent into the IP steam turbine. After the IP steam turbine the steam is mixed with steam from the LP part of the HRSG and led into the LP steam turbine. Finally, when the steam from the LP steam turbine is expanded it is sent to the condenser and then sent back into the HRSG.

4.2. Critical Components Assessment

As it is visible from Figure 4-2, the HRSG has various components. However, the components that are more likely to be critical and, as a result, going to be examined for fatigue damage, are the following:

1. The high pressure drum (HP Drum)
2. The high pressure superheater (HPSH) outlet manifolds
3. The reheater (RHTR) outlet manifolds

The HP Drum has a relatively thick wall which can result in a significant through wall temperature difference and a high thermal stress. The HPSH and RHTR outlet manifolds are subject to the highest temperatures at full load operation, and to the most rapid rates of temperature change during start-up. None of the other components need to be assessed because they have thinner wall and endure much less severe transients than the aforementioned components.

In the following tables the geometry data of the components under investigation, as well as the process details, are shown.

***Table 4-1**: Geometric data for components*

		Main Vessel		Branch/Nozzle	
Component	**Material**	**Out. Diam. [mm]**	**Wall Thick. [mm]**	**Out. Diam. [mm]**	**Wall Thick. [mm]**
HP Drum	SA 299 CC2364	2043	107	390.4	80
HPSH1 Outlet Manifold	SA 335 P91	273.1	50.8	114.3	17.1
RHTR1 Outlet Manifold	SA 335 P91	508	26.18	114.3	8.6

***Table 4-2**: Process data for each of the components for a cold start*

Component	**T_{min} [°C]**	**T_{max} [°C]**	**p_{min} [MPa]**	**p_{max} [MPa]**
HP Drum	10	339.6	0.1	14.5
HPSH1 Outlet Manifold	10	567.1	0.1	14.25
RHTR1 Outlet Manifold	10	566.7	0.1	2.98

The components are going to be examined under a cold start since this is the most severe situation. By implementing the methodology described in the relevant chapters of EN 12952-3 (see Appendix A: Critical components assessment calculations) the following results of the fatigue evaluation for a cold start are obtained and depicted in Table 4-3.

***Table 4-3**: Summary of fatigue evaluation*

Component	**Damage Factor, C**
HP Drum	1.391
HPSH1 Outlet Manifold	0.444
RHTR1 Outlet Manifold	0.017

It can be seen that the HP Drum has a usage factor higher than unity. This suggests that the operation of this component is not in the safe limits. Thus, a more detailed investigation is necessary. However, a similar investigation held by ALSTOM [34] showed the same results for the damage factor of the HP Drum. After implementing a finite element model it was shown that the damage factor is lower than unity, hence safe operation is ensured.

The HPSH1 and RHTR1 outlet manifolds, have a damage factor lower than unity, thus making their operation safe for operation under these conditions. However, for the case of the HPSH outlet manifold, magnetite cracking might occur (see Appendix B).

In the present assessment, only fatigue is taken into account. However, for the case of HPSH1 and RHTR1, due to the higher temperatures, creep might have also an impact. Nevertheless, in this study only fatigue is going to be investigated, hence the component to focus on is the HP Drum.

HP Drum

The HP Drum is a long cylindrical vessel (see Figure 4-3) and it acts as a reservoir of water/steam. The HP Drum stores the steam generated in the evaporator and acts as a phase-separator for the steam/water mixture. The steam-free water is re-circulated with the feedwater to the evaporator for further steam generation. The saturated steam is discharged through a number of outlet nozzles for further heating. In principal, a steam drum also serves to [15]:

1. mix the feedwater with the saturated water remaining after the steam separation,
2. mix the corrosion control and water treatment chemicals (if used),
3. purify the steam to remove contaminants and residual moisture,
4. remove part of the water (blowdown) to control the boiler water chemistry (solids content), and
5. provide limited water storage to accommodate rapid changes in boiler load.

However, the primary function of the steam drum is to permit the effective separation of steam and water. This may be accomplished by providing a large steam-water surface for natural gravity-driven separation or by having sufficient space for mechanical separation equipment.

Some design characteristics of the HP Drum installed in Maxima Power Plant are depicted in the following table:

***Table 4-4**: Design characteristics of the HP Drum*

Data	**Value**
Design pressure (bar)	163
Design temperature (°C)	349
Outside diameter (mm)	2043
Wall thickness (mm)	107
Drum length (mm)	12192
Material Properties[1]	
Material	SA299 (CC2364)
Thermal conductivity (W/mK)	52
Coefficient of linear thermal expansion (K^{-1})	1.44E-05
Poisson's ratio	0.3
Young's modulus (MPa)	188379
Thermal diffusivity (mm^2/s)	9.449

[1] Provided by GDF Suez and acc. to [15, 37, 38]

Carbon steel plate is the primary material used in drums [15]. SA299, a 517.5 MPa tensile strength material, ordered to fine grain melting practice for improved toughness, is used for heavy section drums (HP Drums), those more than about 101.6 mm in thickness.

***Figure 4-3**: The HP Drum*

4.3. HP Drum Simulation

In this section the simulation model described in the previous sections is applied at the HP Drum. The main inputs of the simulation model are:

- HP Drum wall thickness
- HP Drum inner radius
- Heat conductivity for the material
- Young's modulus
- Thermal diffusivity
- Poisson's ratio
- Coefficient of linear thermal expansion
- Heat transfer coefficient between the fluid and inner surface, h
- Pressure inside the HP Drum as a function of time

4.3.1. Model calibration

Before the simulation, the model has to be calibrated in terms of the heat transfer coefficient. This is necessary, because the fluid inside the HP Drum is a mixture of steam and water and hence it is complicated to choose a single value. By using different heat transfer coefficients the transfer function coefficients are accordingly calculated. Then by comparing the measured

outer temperature (available from plant measurements) with the outer temperature calculated by the model, tuning of the model is possible in terms of heat transfer coefficient.

Figure 4-4, shows the response of the outer temperature by using different values of the heat transfer coefficient compared with the measured outer temperature derived from real plant measurements.

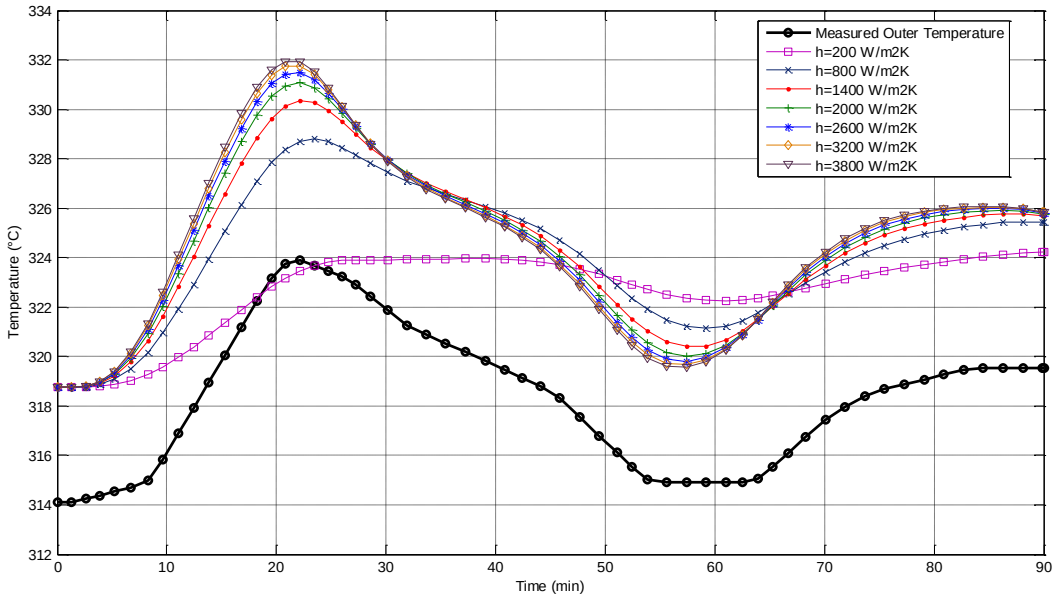

***Figure 4-4**: Calculated outer temperatures using different values of heat transfer coefficient*

Firstly, it can be seen that there is a difference between the measured and the calculated values of approx. $\Delta T=5$ °C. The reason for this difference lies upon the fact that it could be a bias in the measurement of the outer temperature, which is a common phenomenon in measuring systems. Also, another important aspect is the location of the thermocouples for measuring the temperature and the transducers for measuring the pressure. In principle, they have to be located at the same axial coordinate. However, in practice they may have a different position thus making the calculated outer temperature to have a mismatch with the measured data. This has to do with the assumption that has been taken that the temperature is spatially constant in the axial as well tangential direction. Nevertheless, this mismatch introduces an error of around 1.5% which is inside the acceptable region.

Secondly, it is clear that by increasing the value of the heat transfer coefficient, the response of the outer temperature is faster and more accurate. However, for h>2000 W/m^2K the change in response is becoming less significant and for h>3000 W/m^2K the response is almost identical. Hence, a good assumption could be to use a value between 2000 and 3000 W/m^2K.

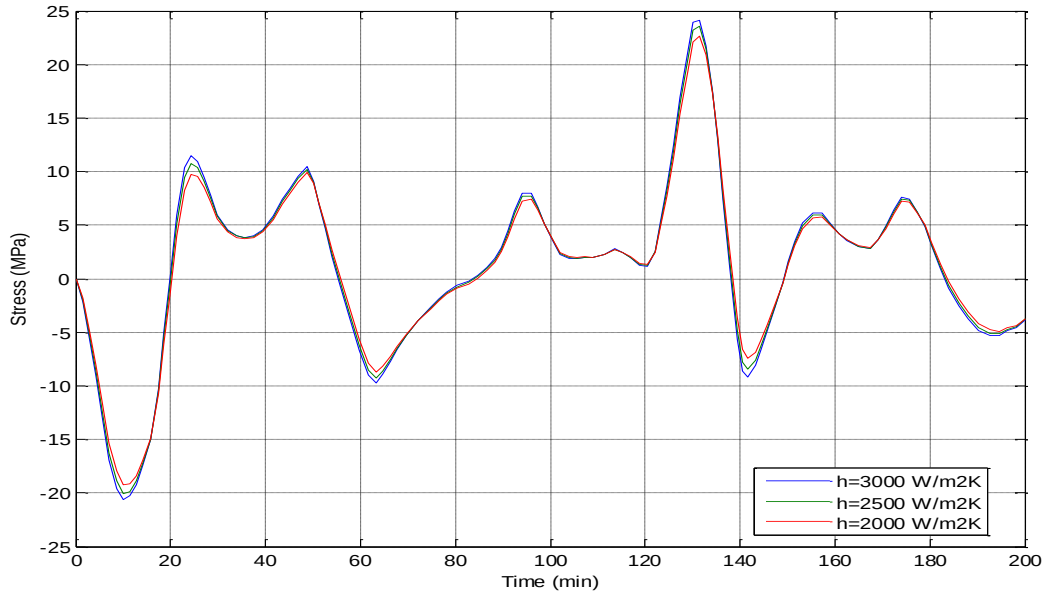

***Figure 4-5**: Corresponding thermal stress using different values of heat transfer coefficient*

Figure 4-5 shows the corresponding thermal stress calculated using different values of the heat transfer coefficient. It can be seen that for 2000 < h < 3000 W/m^{2}K, the impact on the calculation of the thermal stress is not significant. As a result, a good assumption would be to use an average value of 2500 W/m^{2}K. This value has a good agreement with the EN12952-3 norm, where a value of 3000 W/m^{2}K is used for the heat transfer coefficient inside the HP Drum [14].

By running a simulation with h=2500 W/m^{2}K the results depicted in Figure 4-6 are obtained.

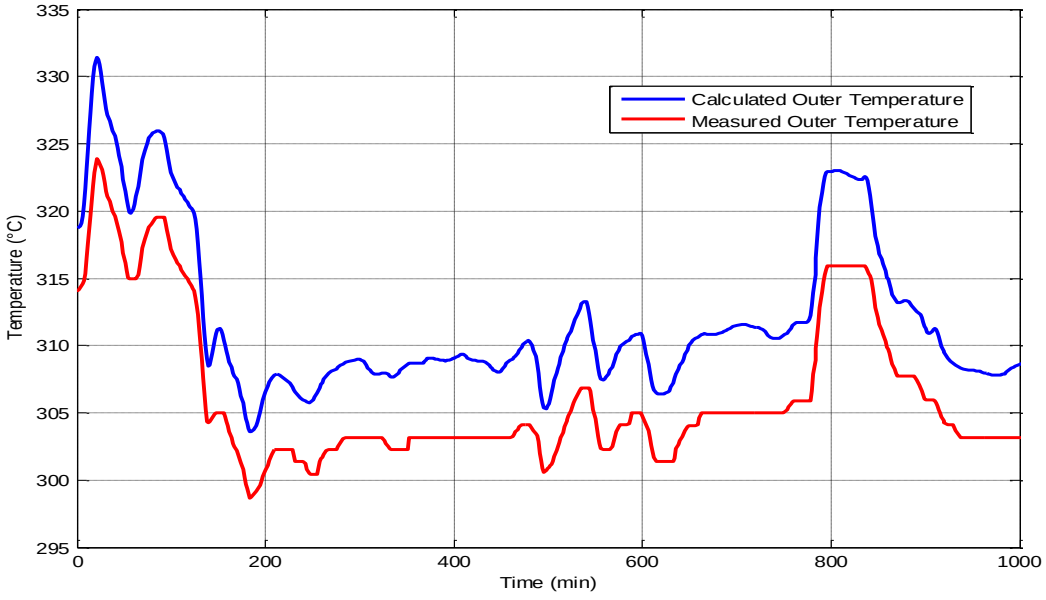

***Figure 4-6**: Calculated outer temperature compared to the measured data*

From this graph it is clear that the response of the calculated (from the model) outer temperature, matches very well the measured data. Also, the aforementioned offset of 5 °C can be identified.

Figure 4-7 shows the response of the temperature at the inner and outer surface according to the fluid temperature changes. It can be seen that the inner surface temperature has a faster response from the outer surface temperature. That is reasonable considering the thickness of the steam drum.

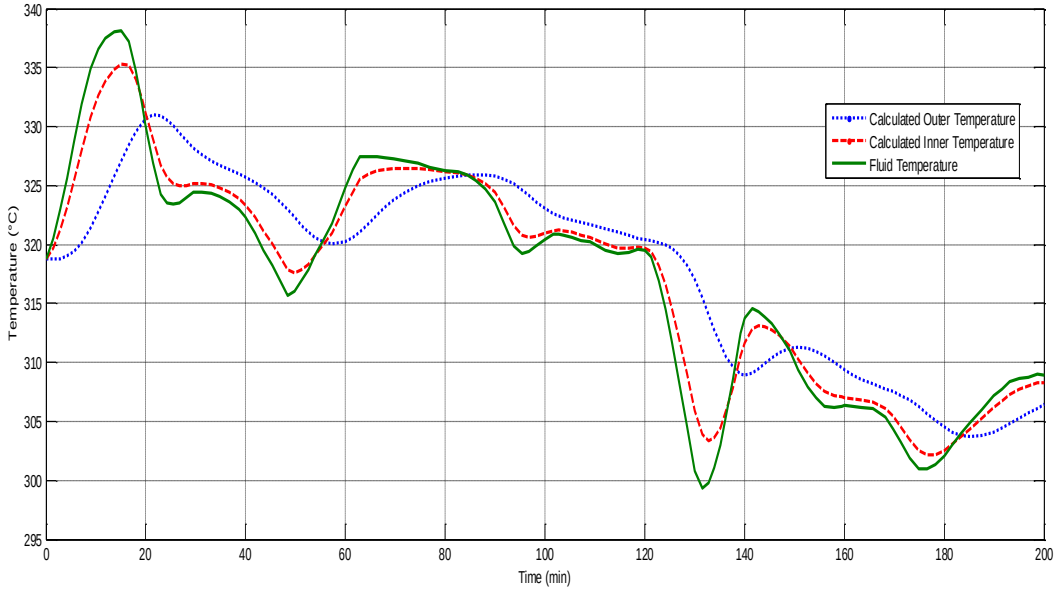

***Figure 4-7**: Temperature response*

After the model is calibrated and the temperature response is within the desirable region, four different transient situations are modeled. For this, four different pressure signals are used. First, a load change operation is simulated where the power output of the plant is continuously changing. Then, a typical 24h operation is simulated in order to depict the effects of daily cycling in modern GTCC's. Finally, a shut down and a start-up process are simulated. In these two situations, the plant parameters are changing more rapidly, hence there is a big interest to estimate the stress evolution.

4.3.2. Load Change

First, a simulation is held for a situation which includes a load change. In the beginning the unit runs on 40% part-load. Then it ramps up to 60% part-load. After a steady state period of approximately 50 min, it ramps up again and after some fluctuations it reaches 100% full load.

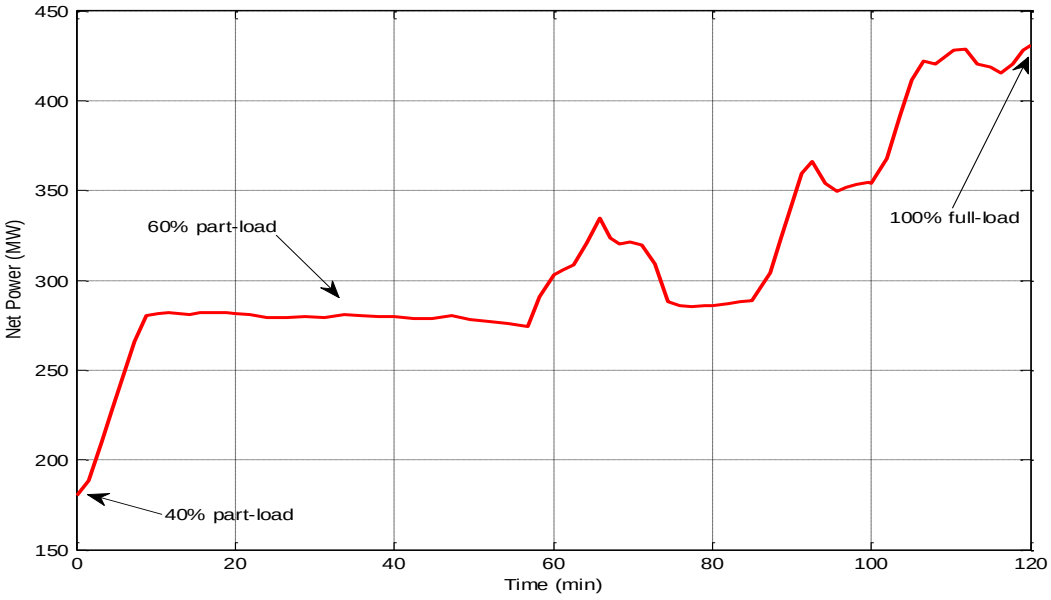

***Figure 4-8**: Net power output of the unit*

The following graph shows the response of the inner and outer temperature as calculated by the model. Moreover, the graph shows the signal of the fluid temperature inside the HP Drum derived from the pressure signal by assuming that the fluid temperature is the saturated temperature. The conversion of the pressure signal into the saturated temperature is done using FluidProp (see Appendix C). Due to the relatively thick wall of the HP Drum, the outer temperature has a delay in the time response from the inner temperature.

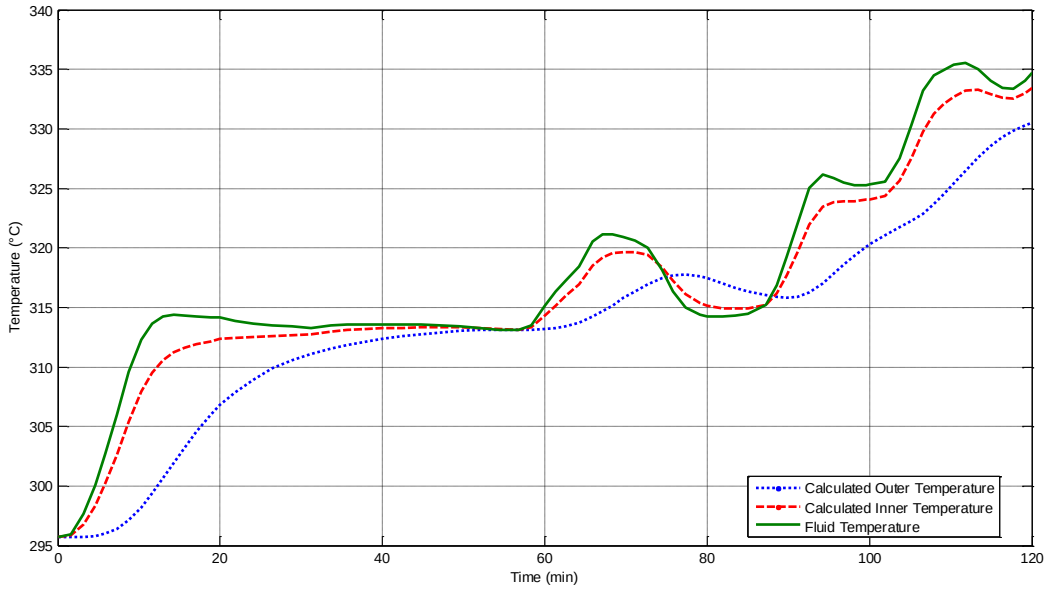

***Figure 4-9**: Fluid, inner and outer surface temperature response*

The next graph shows the corresponding thermal stress. When the temperature increases, the stress becomes compressive and when the temperature decreases the stress becomes tensile. In this situation the stress is mostly compressive since the unit heats up as it increases its load.

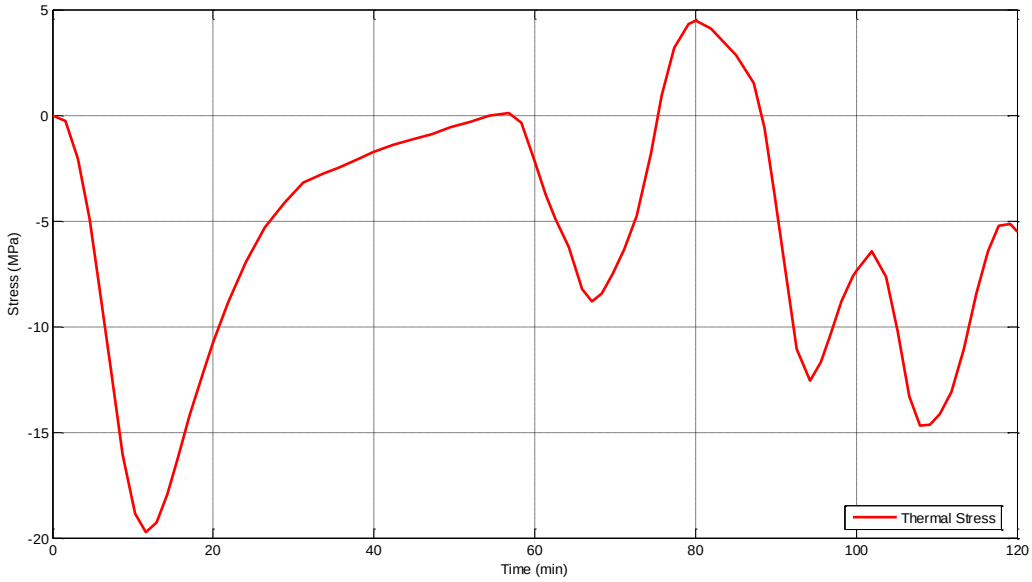

***Figure 4-10**: The thermal stress*

Then by using the formulas mentioned in the previous sections, the mechanical stress is calculated.

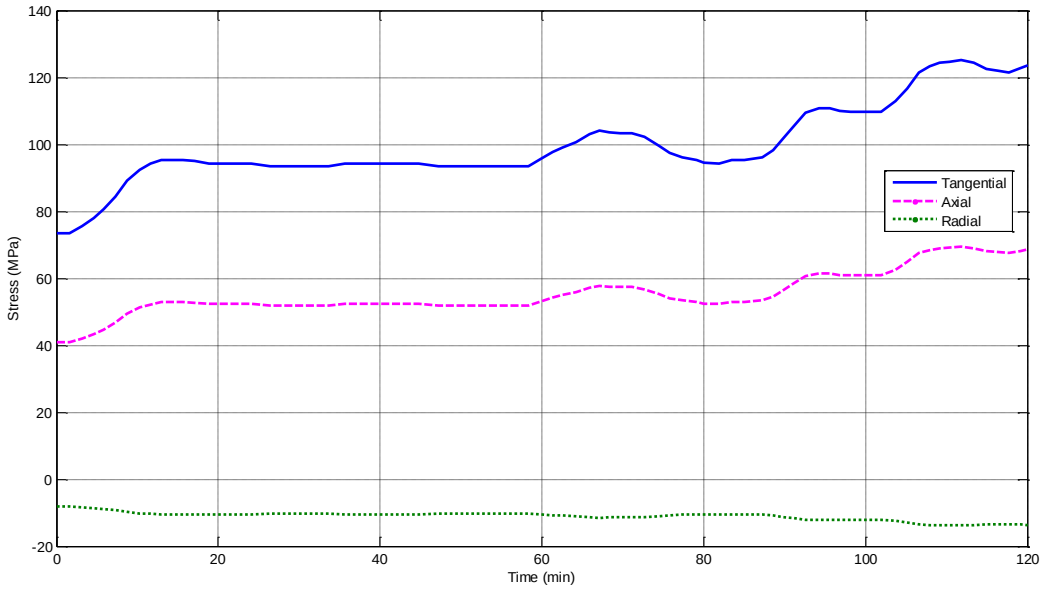

***Figure 4-11**: Principal mechanical stresses*

The combination of the mechanical and thermal stress, gives the principal structural stresses as depicted in the following graph.

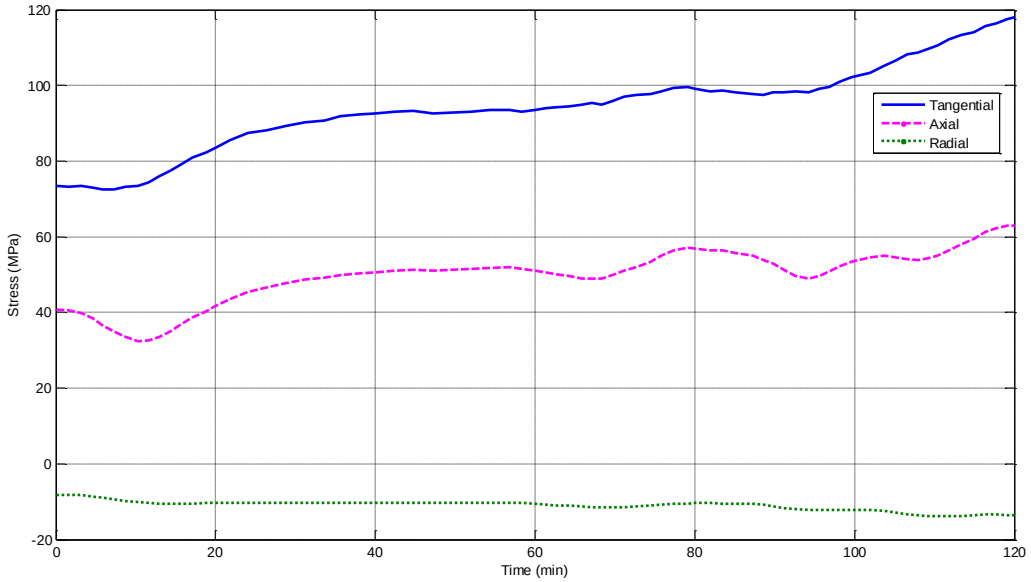

***Figure 4-12**: Principal structural stresses*

It can be seen that the stress in the radial direction are always compressive.

The next graph depicts the evolution of the effective stress using Tresca's and Von Mises criteria. It can be seen from the graph that the Tresca criterion is more conservative than the criterion suggested by Von Mises.

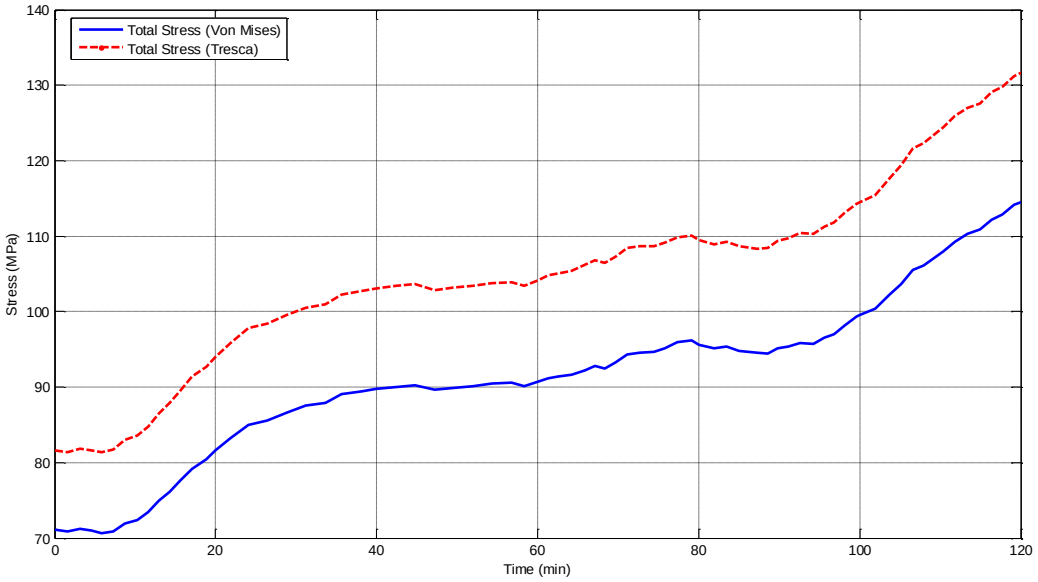

***Figure 4-13**: Equivalent stress*

The next step of the simulation requires the identification of the fatigue cycles using the equivalent stress signal. For this case the equivalent stress signal using the Tresca's criterion was introduced as an input to the rainflow algorithm. The extracted fatigue cycles are depicted in Figure 4-14. In addition, Table 4-5 shows the computed values for each identified cycle.

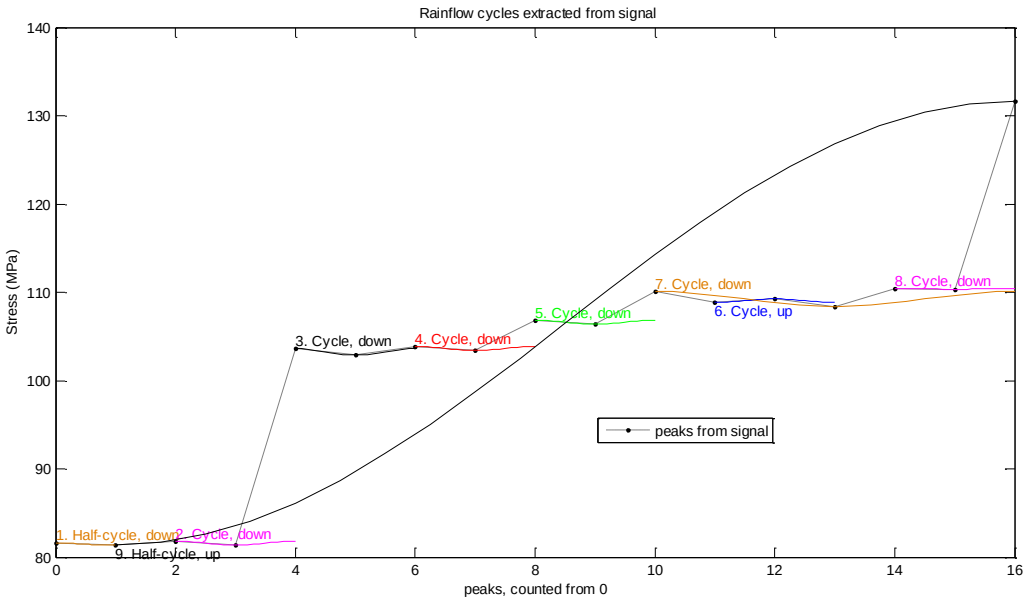

***Figure 4-14**: Extracted fatigue cycles form stress signal*

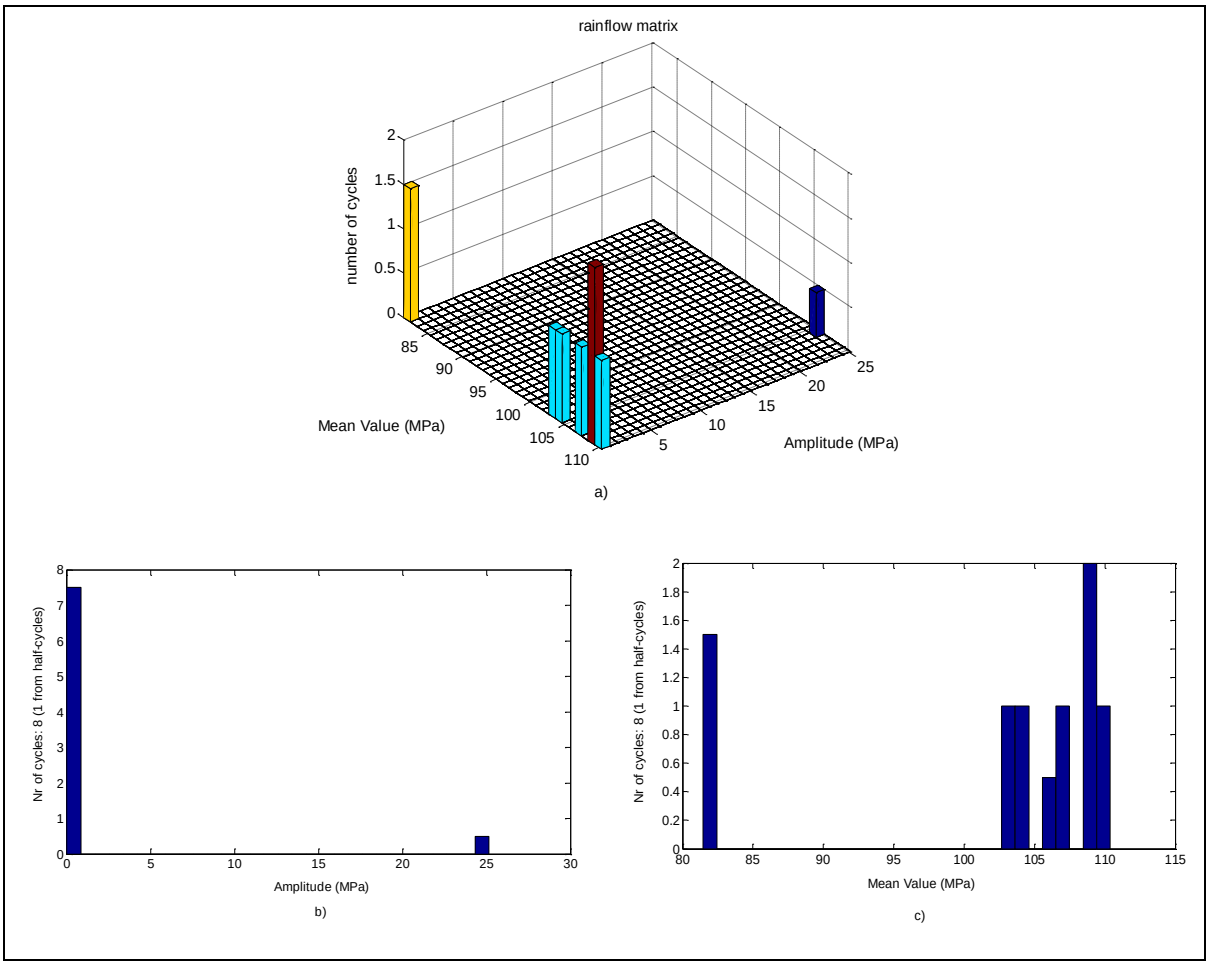

***Figure 4-15**: a) Rainflow matrix b) Rainflow Amplitude and c) Rainflow Mean Value*

***Table 4-5**: Results of the rainflow counting for each cycle*

Number of the cycle or half-cycle	C1	C2	C3	C4	C5
Amplitude $\Delta\sigma/2$ (MPa)	0.1313	0.2110	0.3741	0.2200	0.1944
Mean value σ_m (MPa)	81.4669	81.5881	103.262	103.6448	106.6156
Cycle or half-cycle	0.5	1	1	1	1
Number of the cycle or half-cycle	**C6**	**C7**	**C8**	**C9**	
Amplitude $\Delta\sigma/2$ (MPa)	0.1848	0.8570	0.0278	25.1552	
Mean value σ_m (MPa)	109.0589	109.2398	110.376	106.4908	
Cycle or half-cycle	1	1	1	0.5	

According to the results from the rainflow counting, the fatigue cycles have a rather small amplitude which is much less than the yield strength at the reference temperature (250.8 MPa), leading to a high-cycle fatigue situation. With these small stress amplitudes, the number of cycles to failure could be infinite. A more interesting situation could be a shut down or a start-up process where the changes in the system parameters (temperature, pressure) become more rapidly.

4.3.3. Typical 24h operation

The following graphs show a simulation done for a daily 24h operation. Figure 4-16 depicts the response of the fluid temperature, the inner and outer surface temperatures as calculated by the model.

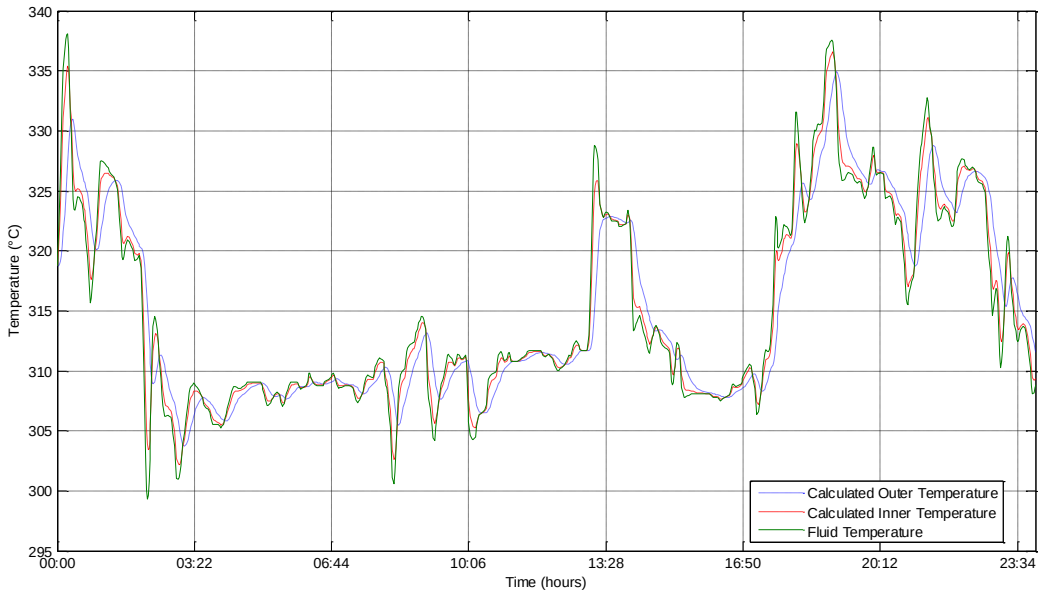

***Figure 4-16**: Temperature response*

It is clear that the plant is continuously in a cycling operation mode. This of course leads to the evolution of thermal stress as seen in Figure 4-17.

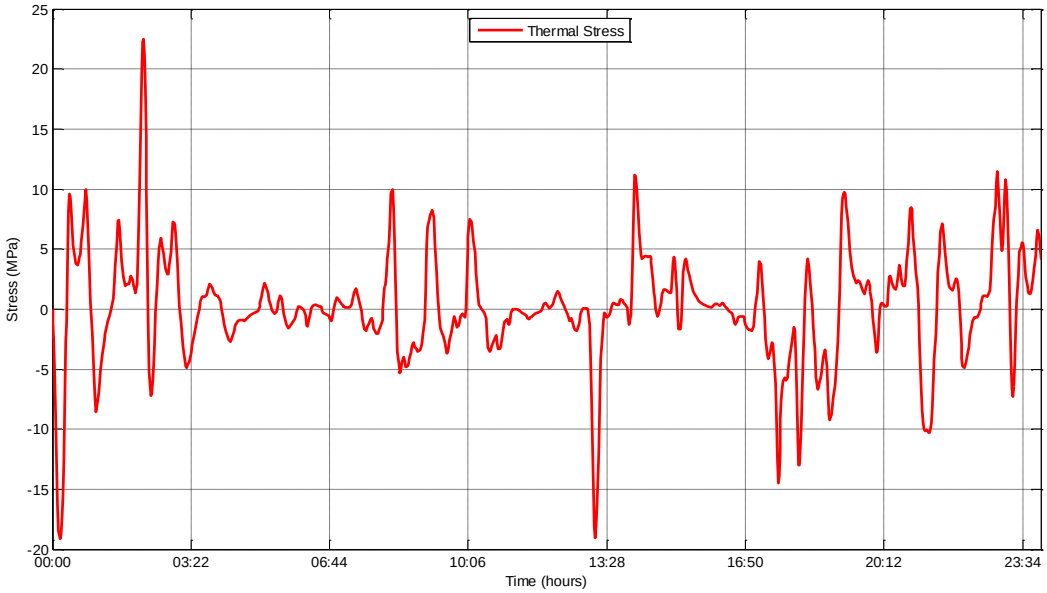

***Figure 4-17**: Thermal stress in a 24h operation*

The evolution of the principal structural stresses is depicted in Figure 4-18.

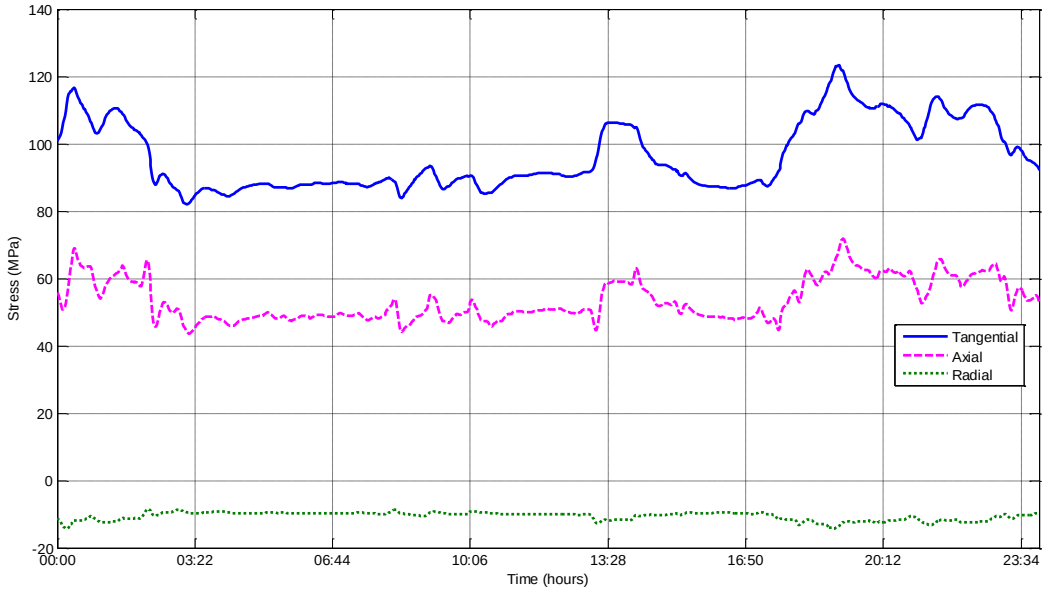

***Figure 4-18**: Principal structural stresses*

In Figure 4-19 the equivalent stress as it is defined by Von Mises and Tresca is plotted. It is clear that during a normal 24h operation fatigue cycles occur due to the cycling activity of the plant.

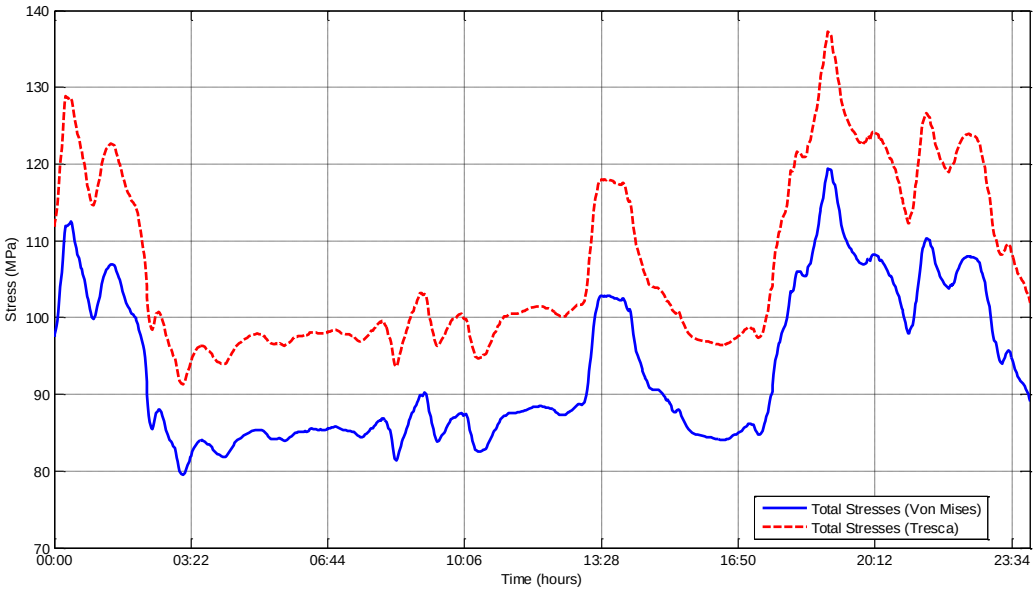

***Figure 4-19**: Equivalent stress in a 24h operation*

Next, the rainflow algorithm is implemented in the Tresca equivalent stress. Figure 4-20, shows the identified fatigue cycles whereas in Table 4-6 the amplitudes and mean values for each cycle are tabulated.

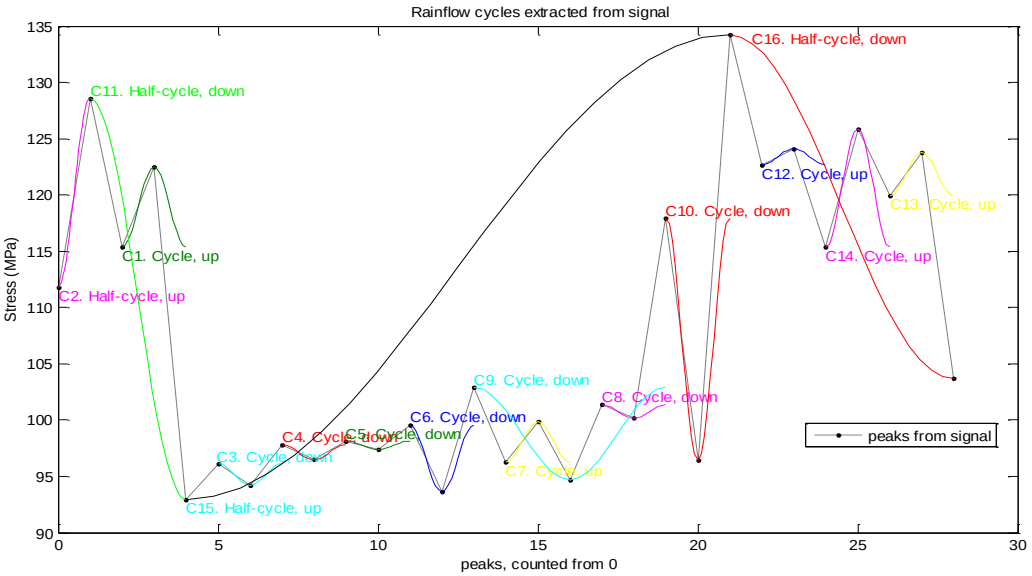

***Figure 4-20**: Extracted fatigue cycles form stress signal*

***Table 4-6**: Results of the rainflow counting for each cycle*

Number of the cycle or half-cycle	C1	C2	C3	C4	C5
Amplitude $\Delta\sigma/2$ (MPa)	3.5589	8.3855	0.9590	0.6689	0.3886
Mean value σ_m (MPa)	118.9147	120.1987	95.1745	97.1566	97.7585
Cycle or half-cycle	1	0.5	1	1	1

Number of the cycle or half-cycle	C6	C7	C8	C9	C10
Amplitude $\Delta\sigma/2$ (MPa)	2.9574	1.7681	0.5968	4.1014	10.7541
Mean value σ_m (MPa)	96.5851	98.0664	100.759	98.8114	107.2023
Cycle or half-cycle	1	1	1	1	1
Number of the cycle or half-cycle	**C11**	**C12**	**C13**	**C14**	**C15**
Amplitude $\Delta\sigma/2$ (MPa)	17.8190	0.7119	1.9045	5.2317	20.6353
Mean value σ_m (MPa)	110.7653	123.3928	121.839	120.6292	113.5815
Cycle or half-cycle	0.5	1	1	1	0.5
Number of the cycle or half-cycle	**C16**				
Amplitude $\Delta\sigma/2$ (MPa)	15.2561				
Mean value σ_m (MPa)	118.9608				
Cycle or half-cycle	0.5				

Finally, the following graph shows the rainflow results in charts in terms of cycle mean value and amplitude.

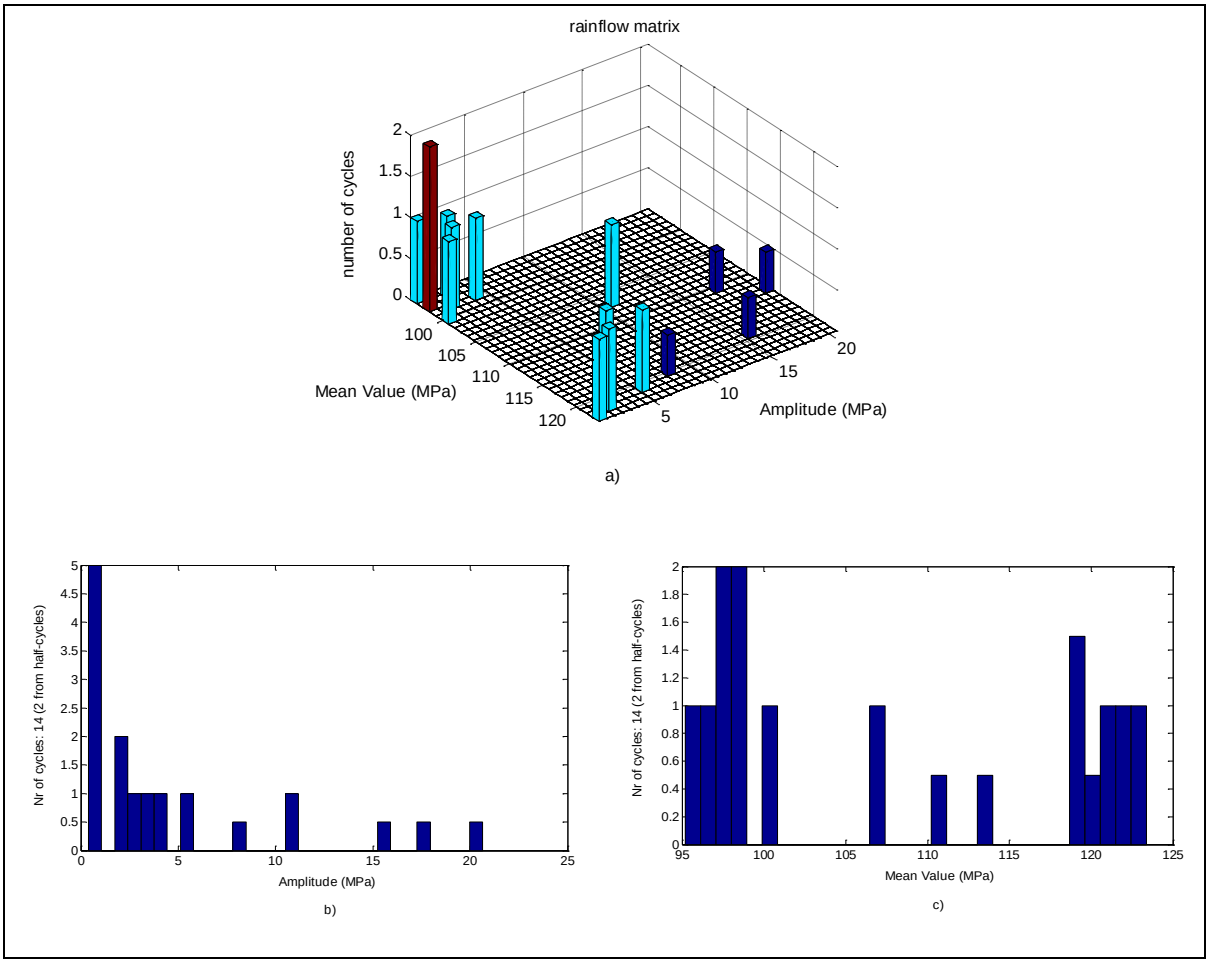

***Figure 4-21**: a) Rainflow matrix b) Rainflow Amplitude and c) Rainflow Mean Value*

Again in this situation the fatigue cycle amplitudes are small leading to high-cycle fatigue.

4.3.4. Shut down

The following graphs depict the temperature and stress response in a shut down process.

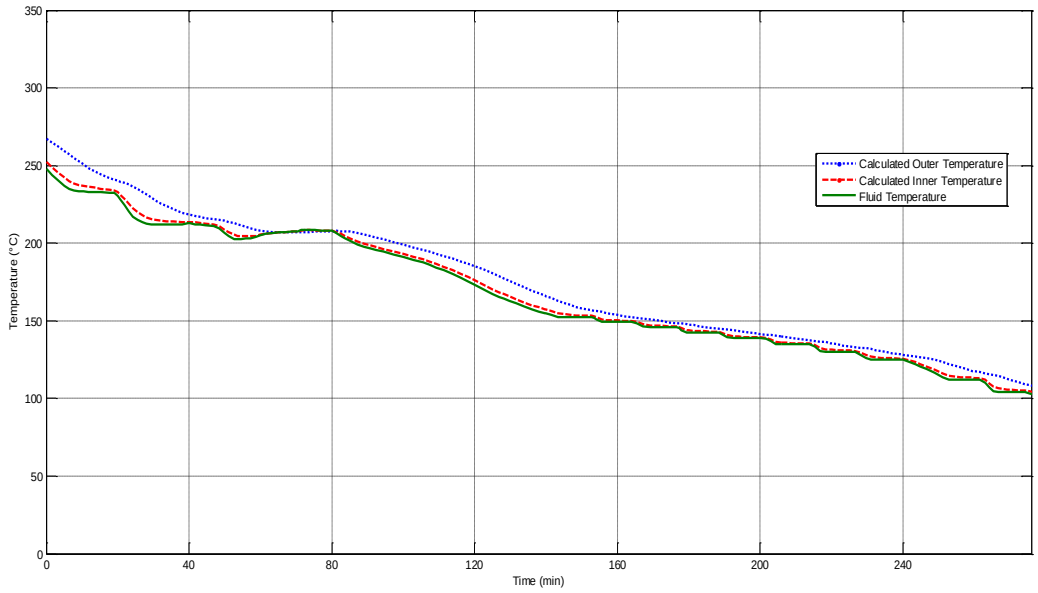

***Figure 4-22**: Temperature response during shut down*

From the above figure it is visible that the shut down process is held in a delicate way in order to avoid the evolution of any excessive stresses. Nevertheless, the following graph shows that still some thermal stress occurs.

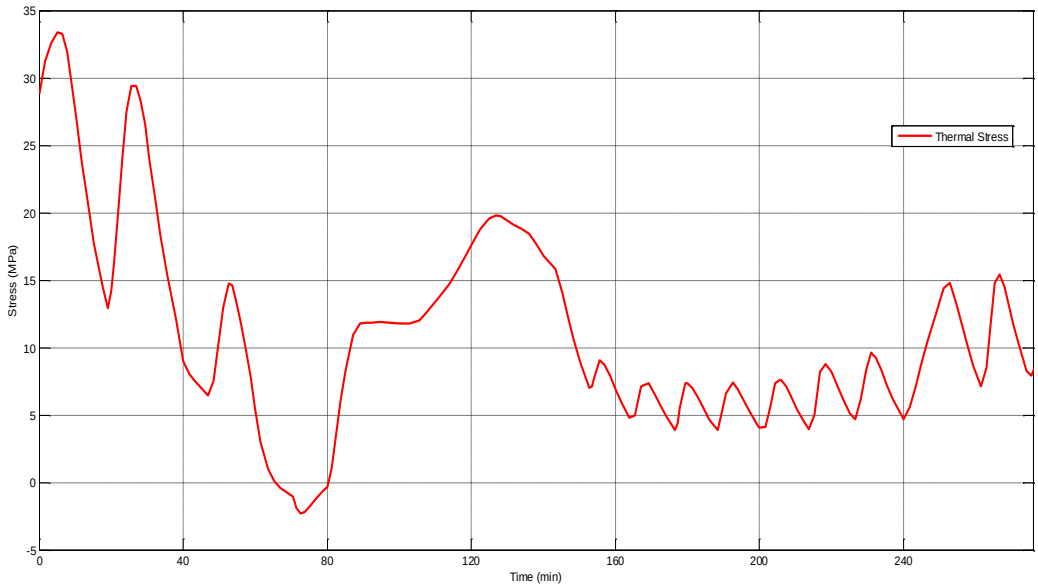

***Figure 4-23**: Thermal stress during shut down*

The next two graphs depict the principal structural stresses and the equivalent stress evolution during a shut down process.

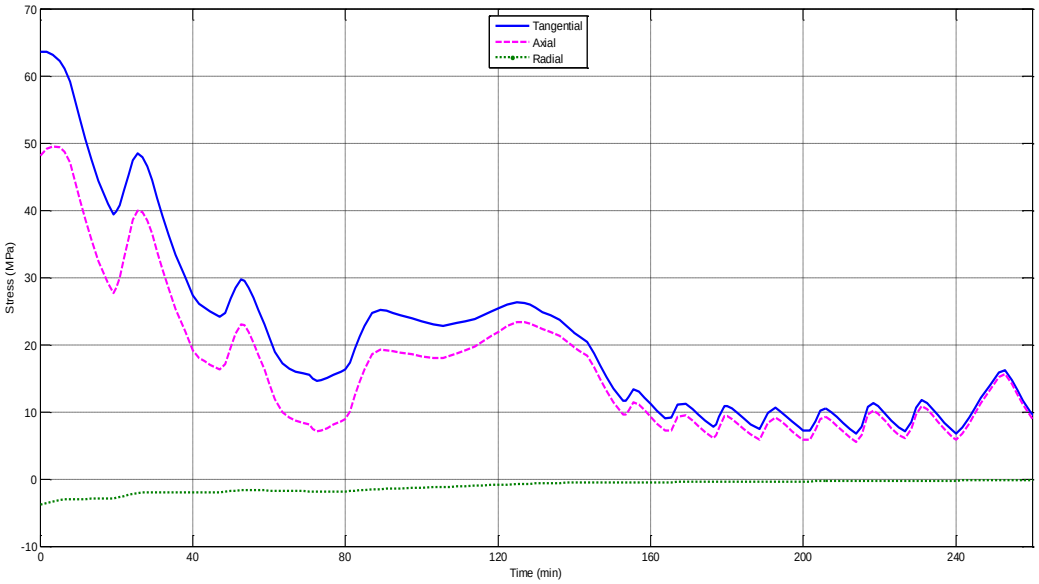

***Figure 4-24**: The principal structural stresses during shut down*

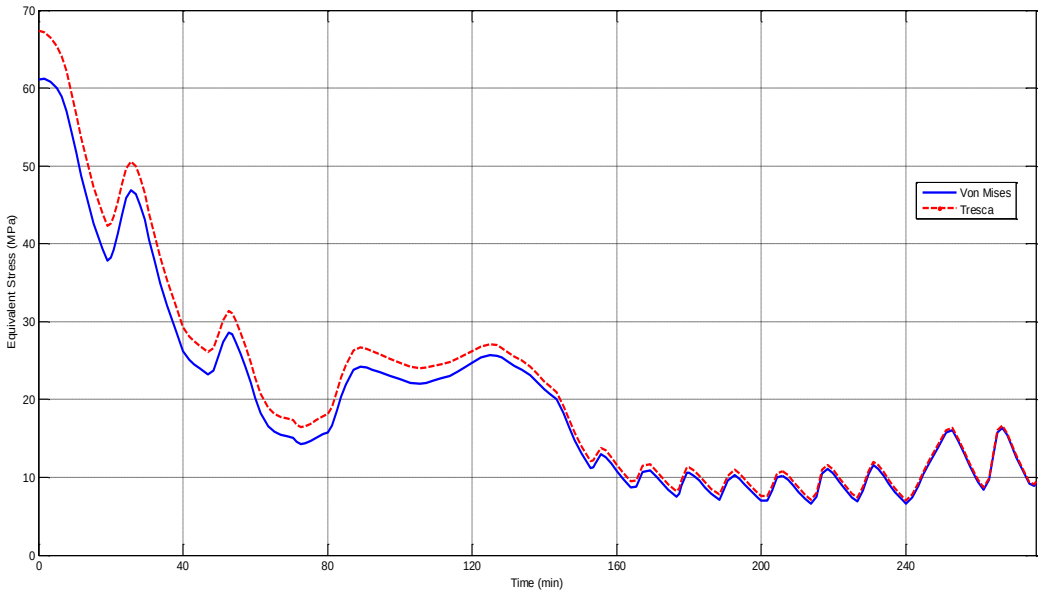

***Figure 4-25**: Equivalent stress during shut down*

As it is observed from the results, the planned shut down is held in a gently way in order to avoid the evolution of any excessive stresses.

The implementation of the rainflow algorithm derives the following results for the identified fatigue cycles.

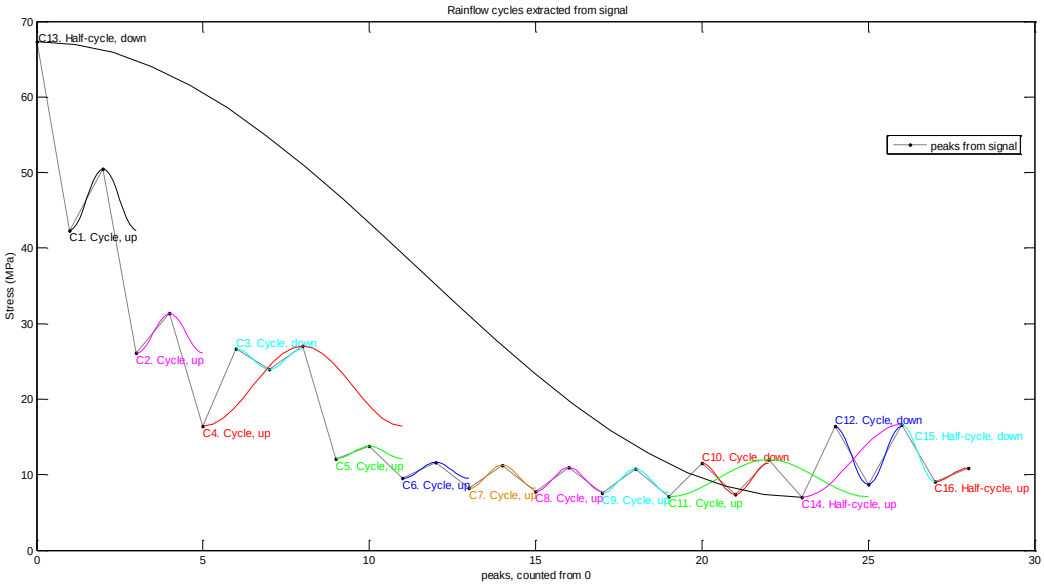

***Figure 4-26**: Extracted fatigue cycles from stress signal*

As it can also be seen from the equivalent stress response, at the second half of the shut down process there is an alternating heat-up and cool-down which results in some additional fatigue cycles making the total number of fatigue cycles 14. However, as it is shown in the following table, these additional fatigue cycles have a very small stress amplitude which would not affect in a significant way the fatigue lifetime, since their value is much lower than the yield strength of the material. The following table shows in detail the data for each identified fatigue cycle.

***Table 4-7**: Results of the rainflow counting for each cycle*

Number of the cycle or half-cycle	**C1**	**C2**	**C3**	**C4**	**C5**
Amplitude $\Delta\sigma/2$ (MPa)	4.0911	2.6145	1.3489	5.3047	0.8334
Mean value σ_m (MPa)	46.4274	28.7164	25.3333	21.7547	12.9462
Cycle or half-cycle	1	1	1	1	1
Number of the cycle or half-cycle	**C6**	**C7**	**C8**	**C9**	**C10**
Amplitude $\Delta\sigma/2$ (MPa)	1.0661	1.5417	1.5700	1.6009	2.0642
Mean value σ_m (MPa)	10.5801	9.7456	9.3743	9.1791	9.4811
Cycle or half-cycle	1	1	1	1	1
Number of the cycle or half-cycle	**C11**	**C12**	**C13**	**C14**	**C15**
Amplitude $\Delta\sigma/2$ (MPa)	2.4381	3.8562	30.1591	4.7916	3.7708
Mean value σ_m (MPa)	9.5438	12.5199	37.1980	11.8305	12.8514
Cycle or half-cycle	1	1	0.5	0.5	0.5
Number of the cycle or half-cycle	**C16**				
Amplitude $\Delta\sigma/2$ (MPa)	0.9074				
Mean value σ_m (MPa)	9.9881				
Cycle or half-cycle	0.5				

Finally, the following graphs show the rainflow results in charts in terms of cycle mean value and amplitude.

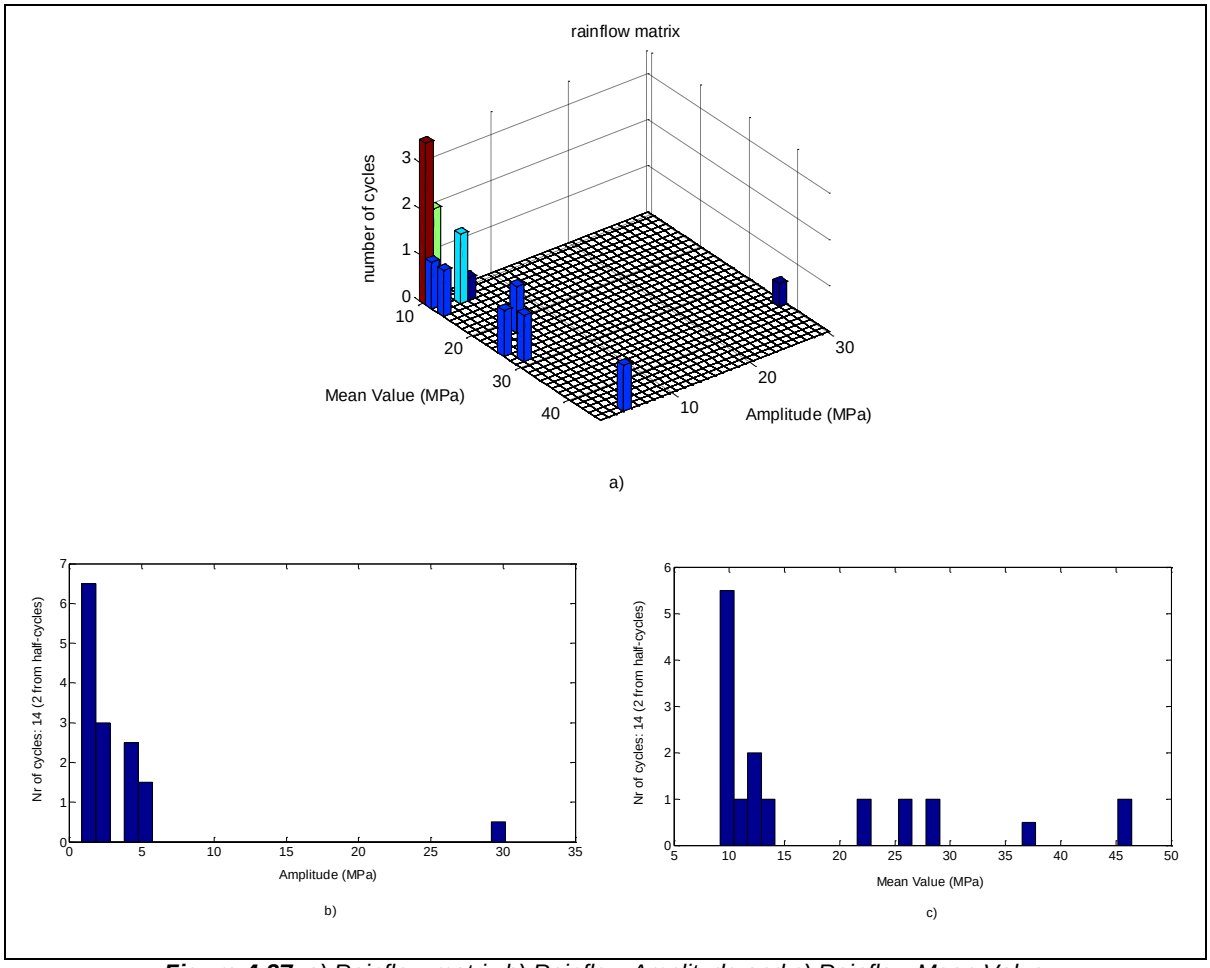

***Figure 4-27**: a) Rainflow matrix b) Rainflow Amplitude and c) Rainflow Mean Value*

4.3.5. Start-up

The following graphs depict the simulation results for a start-up process as it can be identified from real plant measurement data. As it can be seen from the temperature response, the start-up is held according to the power demand, hence after a first rapid increase, which yields some stresses, the temperature is steadily increased and the full power output is reached after more than 4 hours of operation.

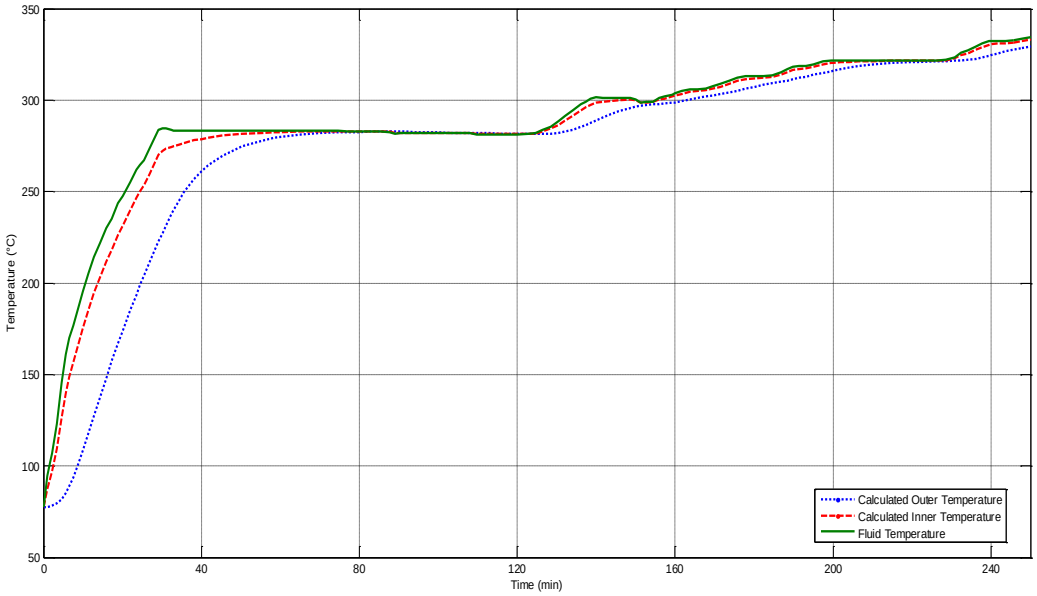

***Figure 4-28**: Temperature response during start-up*

It is obvious from the above graph that the temperature increases rapidly the first 30 min and then it stays constant for approximately 1.5 hr. This rapid temperature increase yields thermal stress as it is seen in the following graph. Also, the period where the temperature remains constant helps to avoid the evolution of larger thermal stress.

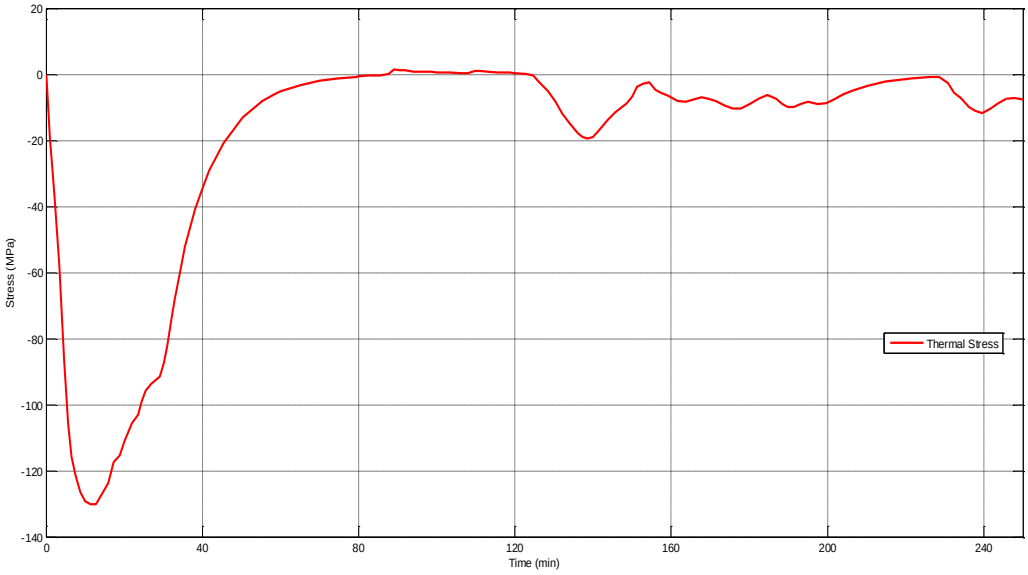

***Figure 4-29**: Thermal stress evolution during start-up*

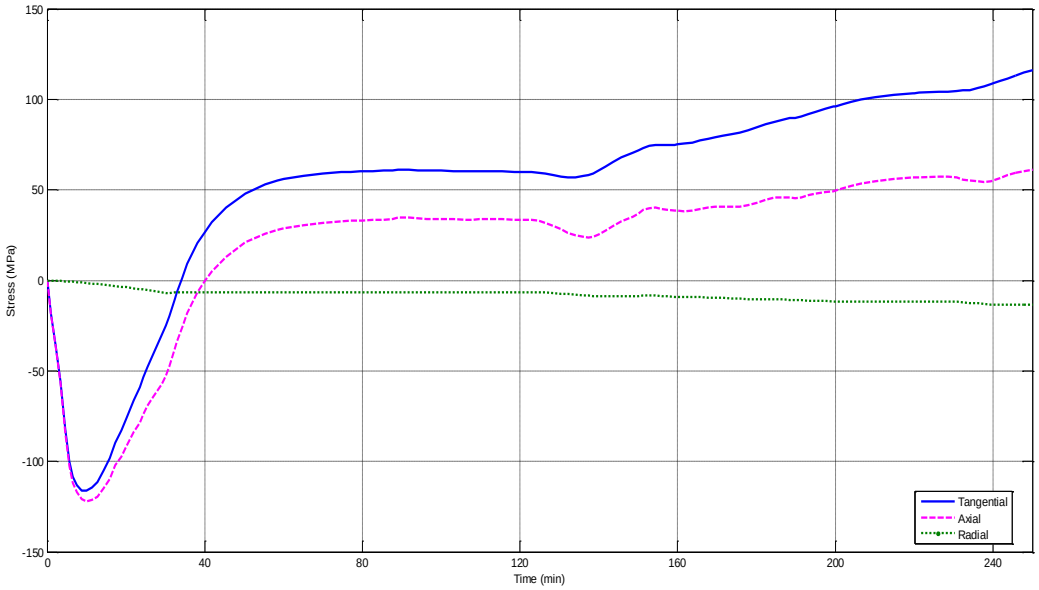

***Figure 4-30**: The principal structural stresses during start-up*

In Figure 4-30, the evolution of the principal structural stresses is depicted. It can be seen that the radial stress is always compressive, whereas the tangential and axial stresses are compressive in the beginning and at some point they become tensile. This behavior is in accordance with the results reported by Bracco in [13] (Figure 4-31) for a start-up process.

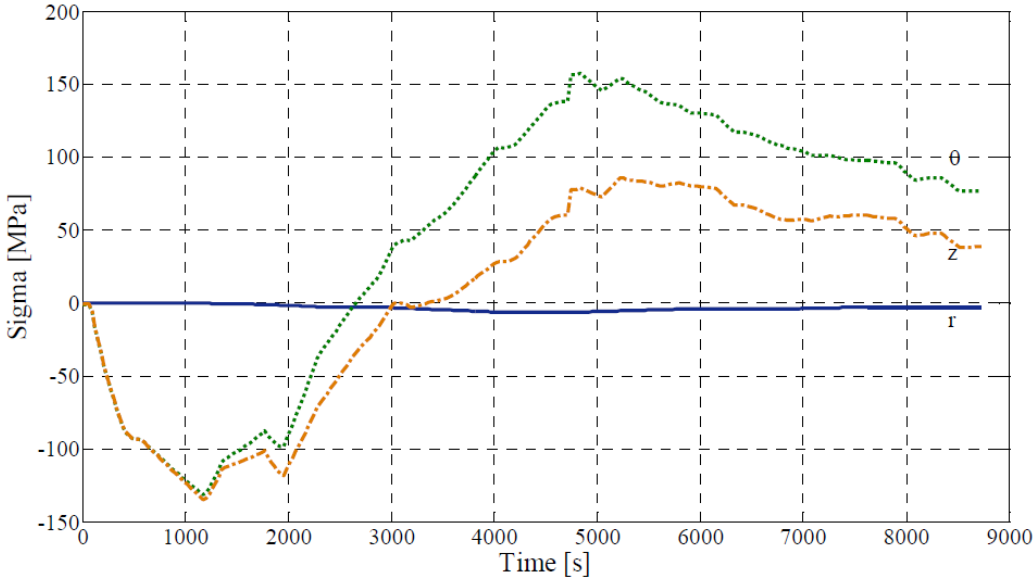

***Figure 4-31**: The principal structural stresses during a cold start-up as reported in [13]*

By applying the Tresca and Von Mises stress criteria, the following results are obtained for the equivalent stress.

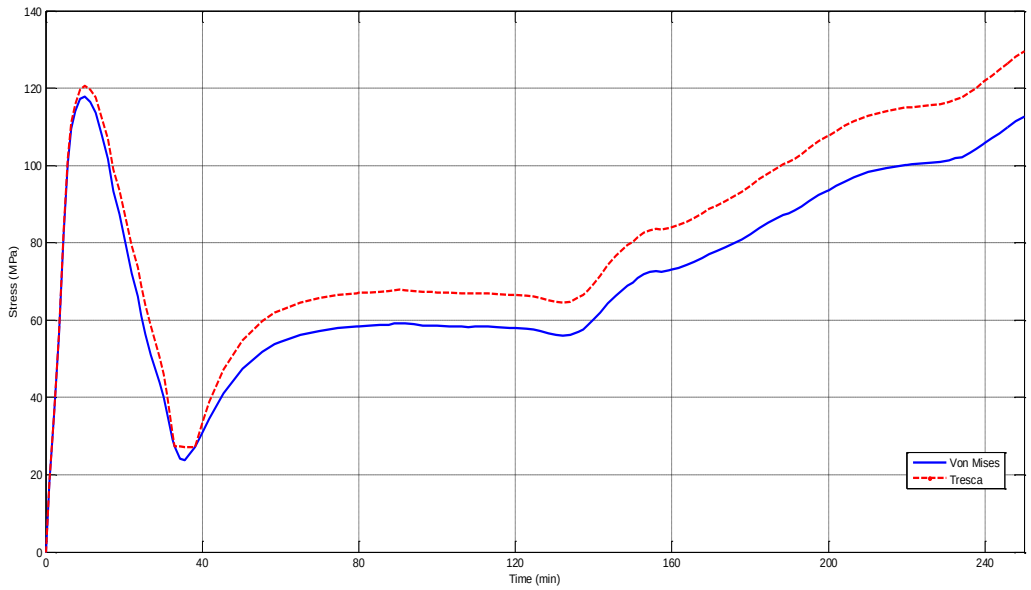

***Figure 4-32**: Equivalent stress evolution during start-up*

Finally, the implementation of the rainflow algorithm gives the following results for the identified fatigue cycles.

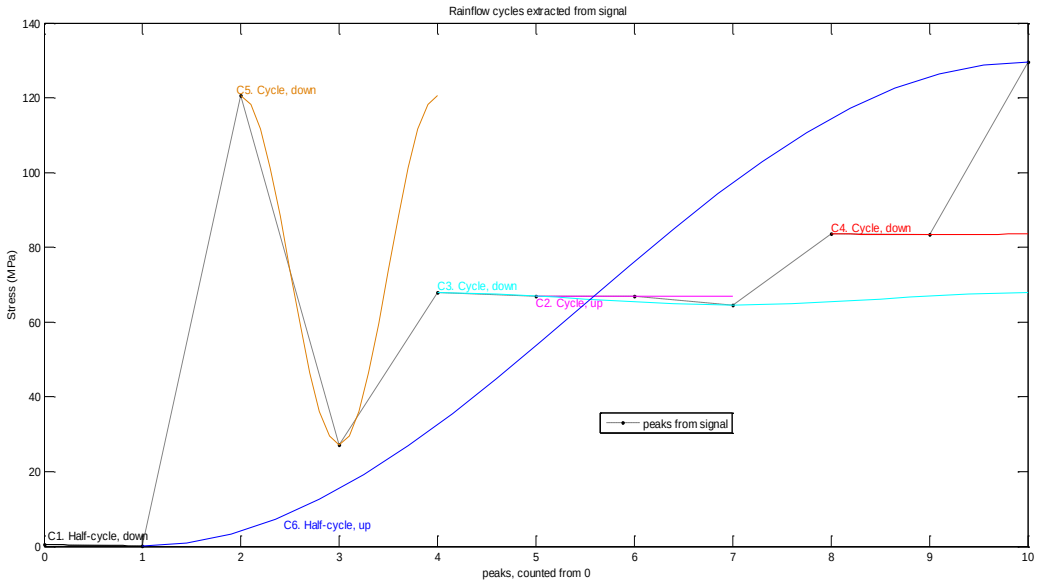

***Figure 4-33**: Extracted fatigue cycles from stress signal for a start-up*

***Table 4-8**: Results of the rainflow counting for each cycle*

Number of the cycle or half-cycle	C1	C2	C3	C4	C5	C6
Amplitude $\Delta\sigma/2$ (MPa)	0.1262	0.0648	1.6453	0.0304	46.6934	64.7277
Mean value σ_m (MPa)	0.3027	66.8834	66.2059	83.5038	73.9040	64.9042
Cycle or half-cycle	0.5	1	1	1	1	0.5

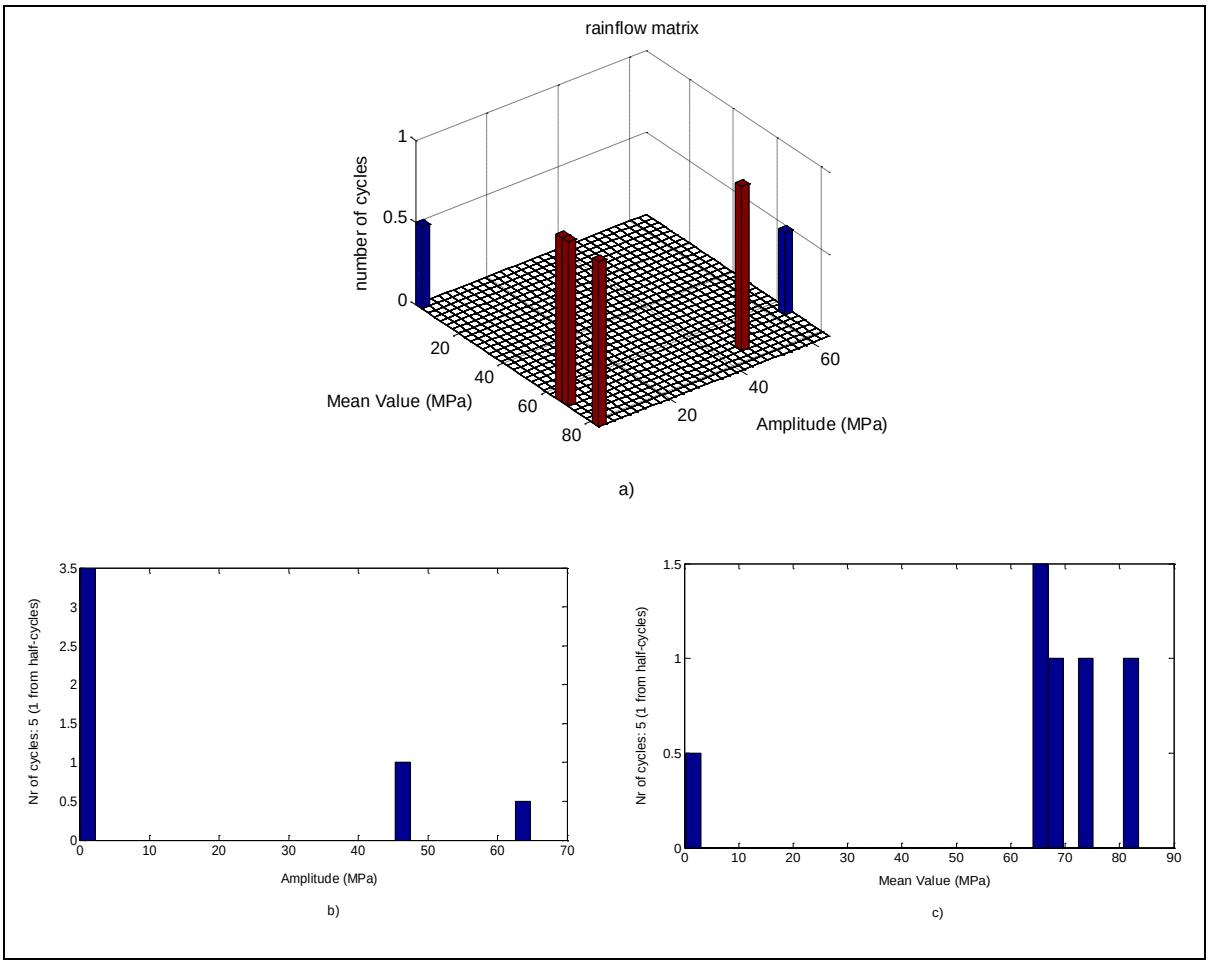

***Figure 4-34**: a) Rainflow matrix b) Rainflow Amplitude and c) Rainflow Mean Value*

The results of the rainflow algorithm show that the start-up process is the most severe, since it yields higher stresses. In the following chapter, the results of the simulation are further discussed.

4.4. Discussion

In all four simulation scenarios, a cycling operation of the unit is identified. This depicts the current trend of the electricity market as it is discussed in the introductory section of this study. It is important to mention that the plant measurements used to derive the stress signal are dated from 2012 and early 2013, hence the findings of the simulation are very recent and up to date.

However, despite the cycling operation of the unit, the implementation of the rainflow algorithm showed small amplitude values of the fatigue cycles. The yield strength of the material at the reference temperature is 250.8 MPa whereas the highest identified fatigue cycle amplitude is 129.4 MPa. This is mainly due to the way that this particular plant is cycled. Start-ups and shut downs are generally avoided. In a period of more than six months the plant had only one shut down and start-up. This is because the plant is capable of going on a low part-load operation when the electricity demand falls to a minimum and maintaining a reasonable efficiency.

This allows the unit not to perform a shut-down, avoiding further cycling of the plant and eventually avoiding any low-cycle fatigue.

According to the simulation results, the most severe situations is a start-up and a shut down process. During these transient situations, there is a rapid change in the plant parameters such as temperature and pressure, which promote the evolution of thermomechanical stresses. In the next graphs, the developed thermal stress as well as the equivalent stress are compared for the start-up and shut down process respectively.

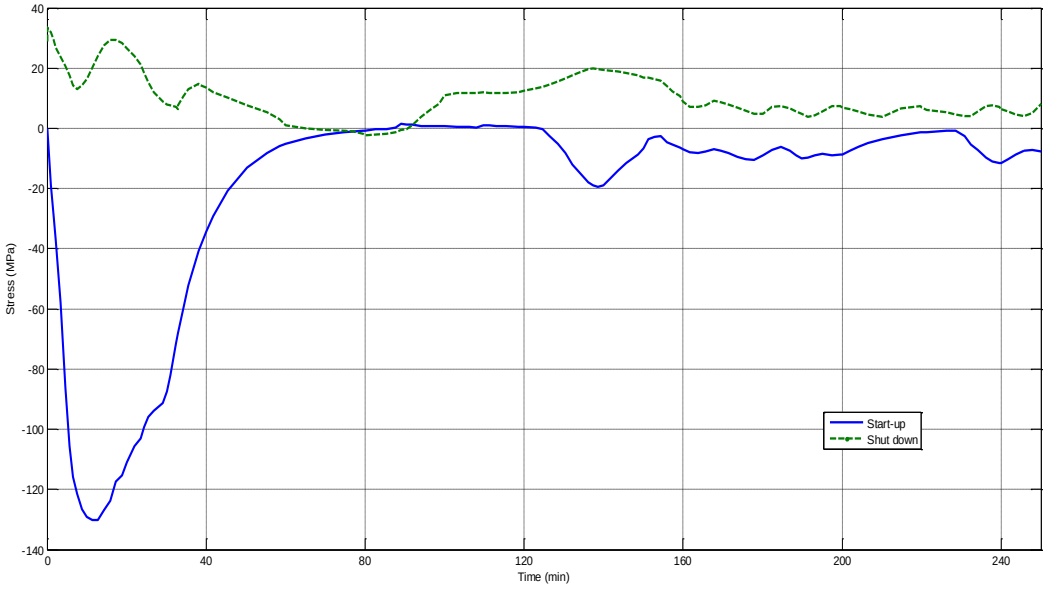

***Figure 4-35**: Evolution of thermal stresses during start-up and shut down*

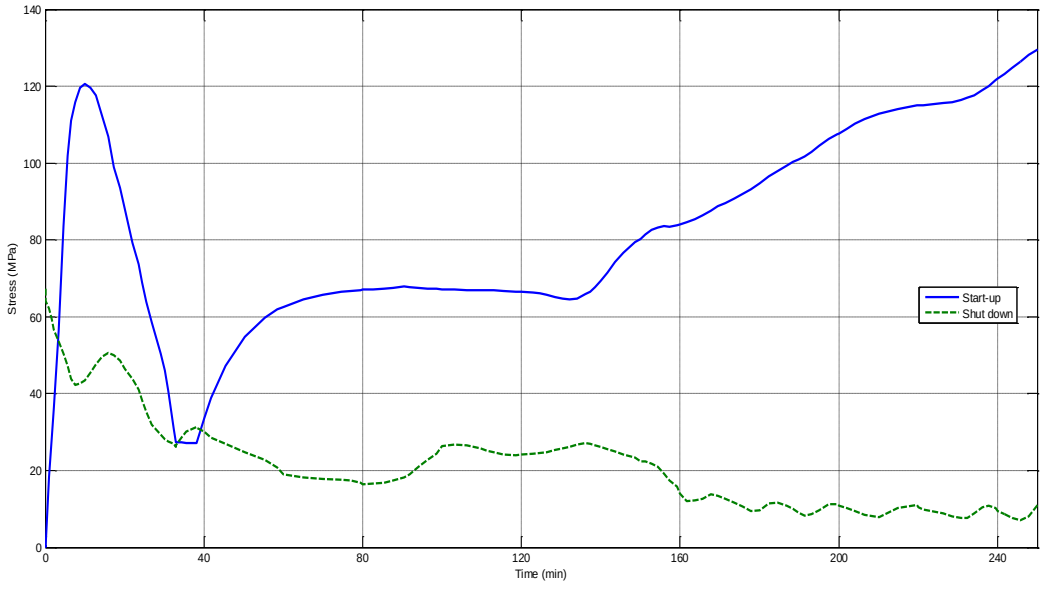

***Figure 4-36**: Equivalent stresses during start-up and shut down*

The start-up seems to be a more intensive process since, as it can be easily seen, higher stresses are developed. The reason for this is the fast temperature increase, especially for the first 30 minutes, of the fluid inside the HP Drum. This of course is a consequence of the very fast

load change of the total unit. Usually, in a start-up situation there is a specific demand in power generation and a fast response to deliver this specific power is a very important criterion for the level of flexibility of the whole plant.

On the other hand, during shut down, where there is no demand in fast power output response, the cooling down is held steadily in order to avoid the evolution of excessive stress.

Nevertheless, it is important to remind the reader that especially for the start-up process certain assumptions have been made which might result in a specific uncertainty (see 3.1 Modeling Assumptions). However, this uncertainty is becoming less important in this simulation, since the start-up is not a cold start-up process.

5. CONCLUSIONS

This study aimed to quantify the consequences of the cycling operation of a GTCC plant in terms of fatigue related wear and tear. The goal was to build a dynamic simulation model capable of calculating the developed thermomechanical stresses in a critical boiler component using on-line plant data and estimate the fatigue lifetime of this particular component.

First, a fatigue assessment was performed in various components of the HRSG using the European Norm EN 12952-3. The outcomes of the assessment showed that the HP Drum has the highest fatigue damage ratio and is thus considered to be the most critical component.

Then, a dynamic model was developed in the MATLAB-Simulink environment and the HP Drum was simulated under different transient operations. These included a load change, a typical 24h operation, a shut down and a start-up.

For each situation the model was able to calculate the temperature response at the inner as well as at the outer surface of the HP Drum. Also the developed thermal stress along with the mechanical stress were estimated at the inner surface. Finally, an equivalent stress was obtained using the thermal and mechanical stresses.

Moreover, using the equivalent stress, a fatigue cycle counting technique (rainflow algorithm), was implemented in order to identify the fatigue cycles and to calculate their peak amplitude and mean value. Depending on the amplitude values, it was possible to identify what kind of fatigue was present (high- or low-cycle fatigue).

The results showed that the plant is continuously cycling as a result of the transient behavior of the current electricity market. In all four transient situations that were simulated, the calculated stress evolution was within the acceptable limits. Even though that fatigue cycles were indeed identified for each scenario, none of them had a peak amplitude greater than the yield strength of the material. The worst case was a start-up process where an amplitude of 129.4 MPa was identified. This was much less than the yield strength at the reference temperature (250.8 MPa). This indicates that only high-cycle fatigue is present.

In terms of fatigue, the lifetime of the HP Drum is not significantly affected by the cycling operation of the plant. This intimates that there is more room for flexibility for the whole unit. However, in order to do so, other critical components need to be investigated in order to obtain safe conclusions.

6. RECOMMENDATIONS

In this final section of the study some recommendations for further research are reported.

- ***HPSH Simulation***

Firstly, it would be of a great interest to expand the model so it can simulate the HPSH outlet manifold. To do this, creep would have to be taken into account since the HPSH experiences much higher temperatures compared to the HP Drum. The HPSH outlet manifold might not have shown a high cumulative fatigue damage (acc. to the critical components assessment), however it is an essential part of the HRSG which experiences high temperature gradients especially in part-load operation.

- ***Plant Simulator***

Moreover, usage of the plant simulator in order to generate a pressure and temperature signal in critical components would be beneficial. This study used only online plant measurements. By using the simulator, a signal can be derived and can be manipulated in terms of rate of temperature change in °C/sec. In this way, the level of flexibility of the plant can be studied and the limits of the ramp-up speeds can be predicted.

APPENDICES

Appendix A: Critical components assessment calculations

Cumulative Fatigue Damage

Practical service conditions often subject many structures to a number of cycles of stress of different magnitudes usually referred as a load cycle. In structural design, the number of repetitions of load assumed to act on a structure during its lifetime is called a load cycle. One method of appraising the damage from repetitive stress to a structure suggested by Miner [17], [16], is that the cumulative damage from fatigue will occur when the summation of the increments of damage equals to unity; i.e.,

$$C = \sum \frac{n}{N} ,$$

Where n is the number of cycles at stress σ and N the number of cycles to failure at same stress σ. N could be determined from σ-n curves for the material (see Figure A - 2).

The damage factor represents the fraction of the total life which is expended by the cycles that occur at a particular stress value. A damage factor less than unity indicates that the component will endure the required cyclic service without risk of cracking.

Input Data

The inputs of the code that must be specified are the following:

- Process Data:
  - p_{min} Lower pressure level of a load cycle (MPa)
  - p_{max} Upper pressure level of a load cycle (MPa)
  - T_{min} Lower temperature of a load cycle (°C)
  - T_{max} Upper temperature of a load cycle (°C)
- Material properties:
  - R_m Tensile strength at room temperature (MPa)
  - R_{et} Yield strength at t* (MPa)
  - β_{Lt} Coefficient of linear thermal expansion at t* (K^{-1})
  - E_t Modulus of elasticity at t* (MPa)
  - D_{th} Thermal diffusivity at t* (mm^2/sec)
  - ν Poisson's ratio
- Component dimensions:
  - e_{ms} Mean wall thickness (mm)
  - d_o Outside diameter (mm)
  - e_{mb} Mean wall thickness of branch (mm)

- ❖ d_{ob} Outside diameter of branch (mm)

- Factors:
  - ❖ h The heat transfer coefficient between internal fluid and metal during transient, (W/m^2K).
  - ❖ C_k Correction factor for taking into account the notch effect associated with surface roughness or welds.
- Cycle Conditions:
  - ❖ ν_t Rate of temperature change in °C /sec. The temperature change varies for different components and under different cycles (hot/cold start, start-up/shut down etc.). A high temperature change means that the plant has a very quick response in load changes, making it flexible, nevertheless this has a big influence in the lifetime of the components in the boiler. Hence, the rate of temperature change is a determining factor for computing the damage factor of different components.
  - ❖ n Number of load cycles to be expected during operation.
- Allowable cycles:
  - ❖ N_A Number of load cycles for crack initiation.
  - ❖ S_s Stress safety factor
  - ❖ S_L Load cycle safety factor

Reference Temperature, t.*

All temperature dependent properties are to be evaluated at t*. The reference temperature t* is calculated from the following formula:

$$t^* = 0.75 \times T_{max} + 0.25 \times T_{min}$$

Stresses

The stresses at the crotch corner at the inner surface of a cylinder or cylinder to sphere intersection are tri-directional. The cyclic stresses considered at this location shall be those due to local temperature difference and pressure. The three principal stresses at the bore are:

$$f_1 = f_{tang} = f_{tang,p} + f_{tang,t}$$

$$f_2 = f_{rad} = -p$$

$$f_3 = f_{ax} = -p$$

Where,

f_1 is the stress tangential to the main body and tangential to the opening, caused by pressure and by temperature difference through the wall

f_2 is the stress radial to the main body; compensating for the fluid pressure at the inside surface of the main body

f_3 is the stress axial to the main body; compensating for the fluid pressure at the inside surface of the opening branch

Considering a cycling boiler operation, the maximum and minimum stress at the bore would be:

$$S_{p,max} = \left(a_m \frac{d_{ms}}{2e_{ms}} + 1\right) p_{max}$$

$$S_{p,min} = \left(a_m \frac{d_{ms}}{2e_{ms}} + 1\right) p_{min}$$

Also, the circumferential (principal) stresses at the inside of the bore caused by through-the wall temperature differences Δt shall be calculated by:

$$S_t = W \times \Delta t$$

Where,

$$W = a_t \frac{\beta_{Lt} E_t}{1 - \nu}$$

$$\Delta t = \frac{\nu_{t1}}{V}$$

$$V = \frac{D_{th}}{\gamma_{cyl} \times e_{ms}^2}$$

$$\gamma_{cyl} = \frac{(u_o^2 - 1)(3u_o^2 - 1) - 4u_o^4 \ln u_o}{8(u_o^2 - 1)(u_o - 1)^2}$$

$$u_o = \frac{d_o}{d_{ms} - e_{ms}}$$

The stress concentration factor due to pressure for openings in cylindrical main body, a_m is calculated as:

$$a_m = 2.2 + e^A \zeta^B$$

Where:

$$A = -1.14\xi^2 - 0.89\xi + 1.43$$

$$B = 0.326\xi^2 - 0.59\xi + 1.08$$

$$\xi = \frac{e_{mb}}{e_{ms}}$$

$$\zeta = \frac{d_{mb}}{d_{ms}} \sqrt{\frac{d_{ms}}{2e_{ms}}}$$

d_{mb} mean diameter of the branch (mm)

d_{ms} mean diameter of main vessel (mm)

The stress concentration factor due to thermal stress is calculated through the following expression:

$$a_t = \sqrt{\left[2 - \frac{h+2700}{h+1700}z + \frac{h}{h+1700}(e^{-7\times z} - 1)\right]^2 + 0.81z^2}$$

Where:

$$z = \frac{d_{mb}}{d_{ms}}$$

Hence, the minimum and maximum stresses are respectively:

$$f_{min} = S_{p,min} + S_{t,min}$$

$$f_{max} = S_{p,max}$$

Protection of the magnetite layer

For boiler components made from ferritic or martensitic steel, which may always or sometimes contain water or water and steam mixtures under normal operating conditions, the magnetite layer on the inside of the components shall be protected by the following additional restrictions:

$$f_{tang,max} = S_{p,max} - p_{max} + 200MPa$$

$$f_{tang,min} = S_{p,max} - p_{max} - 600MPa$$

If the calculated stresses don't meet these restrictions, magnetite cracking might occur hence, new cycle conditions have to be assumed (rate of temperature change) and the calculation should start again.

Cyclic stress range and mean cyclic stress in the case of uniaxial stress

In the case of uniaxial stress state, as depicted in Figure A - 1, the mean cyclic stress shall be determined as:

$$f_v = {}^1/_2\,(f_{min} + f_{max}) = {}^1/_2\,(\check{f} + \hat{f})$$

And the cycling stress range as:

$$2f_{va} = (f_{max} - f_{min}) = (\hat{f} - \check{f})$$

Accordingly the stress amplitude is:

$$f_{va} = \frac{2f_{va}}{2}$$

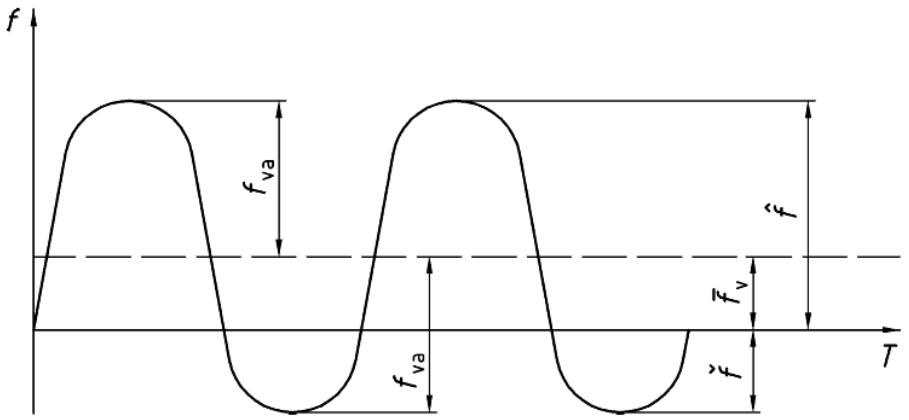

***Figure A - 1**: Stress variation in the case of uniaxial stress (Source: EN12952-3 [14])*

Cyclic stress range and mean cyclic stress shall be increased to account for the notch effect (micro notch effect) associated with surface and weld influences. The notch effect has to do with the increase of the stress in an area of the component near a crack, depression etc. or where there is a change in section such as a sharp angle. This stress increase can be enough to cause failure of the component although the calculated average stress may be quite safe.

The governing factor in each case is the final state following manufacture. The corrected cyclic stress range shall be determined using:

$$2f_{va}^{*} = 2f_{va} \times C_k$$

And the corrected mean cyclic stress using:

$$f_v^{*} = f_v \times C_k$$

The correction factor C_k should be determined by the equation:

$$C_{k0} = \min\{1 - 4.6 \times 10^{-4} \times R_m + 2.3 \times 10^{-4} \times R_m \times \log N_A\,, 1 + 10^{-3} \times R_m\}$$

The value $C_{k0} = 1$ shall be used for calculating the influence of the surfaces in the non-welded region of a component having roughness depths $R_z < 6\ \mu m$, such as can be achieved by grinding or machining.

Controlling stress range

After estimating the stress range $2f_{va}^{*}$, it is important to compare it with the stress range $2f_a$. $2f_a$ is the stress range in an unnotched bar specimen which, for a certain number of load cycles $n = N_A$, produces an 'incipient crack'[2], thus $2f_a$ is used as the permissible stress range.

[2] An incipient crack is a material separation which can be detected with optical aids or non-destructive testing methods.

- Elastic Range:

  If $f_v^* + \frac{2f_{va}^*}{2} \leq R_{et}$, then the stress range $2f_a^*$ shall be determined using the corrected range of the equivalent stress $2f_{va}^*$ and the corrected mean value f_v^* of the range of the equivalent stress in the following equation:

$$2f_a^* = \frac{2f_{va}^*}{1 - \left(\frac{f_v^*}{R_m}\right)^2}$$

  This equation takes into account the modifying influence of the medium stress on the fatigue strength.

- Partly Plastic Range:

  If $f_v^* + \frac{2f_{va}^*}{2} > R_{et}$ and $\frac{2f_{va}^*}{2} \leq R_{et}$, then also the equivalent stress $2f_{va}^*$ is calculated by the equation:

$$2f_a^* = \frac{2f_{va}^*}{1 - \left(\frac{f_v^*}{R_m}\right)^2}$$

  However, in this case the lowered medium stress

$$f_{vR}^* = R_{et} - \frac{2f_{va}^*}{2}$$

  shall be applied instead of f_v^*.

- Fully Plastic Range:

  If the corrected cyclic stress range exceeds twice the yield point $\frac{2f_{va}^*}{2} > R_{et}$, the mean cyclic stress shall be taken as $f_v = 0$ and the controlling stress range $2f_a^*$ shall be determined as a function of the yield point from:

$$2f_a^* = \frac{(2f_{va}^*)^2}{2R_{et}}$$

Correction factor for temperature influence

In the case of a load-cycle temperature $t^* \geq 100\ ℃$, the reduction in fatigue strength caused by the temperature shall be taken into account by means of a correction factor C_{t^*}.

The correction factor should be determined over the temperature range $100\ ℃ \leq t^* \leq 600\ ℃$ using:

$$C_{t^*} = 1.03 - 1.5 \times 10^{-4} t^* - 1.5 \times 10^{-6} t^{*2} \text{ (for ferritic steel)}$$

Consequently, the virtual controlling stress range $2f_{at^*}^*$ shall be obtained as follows:

$$2f_{at^*}^* = \frac{2f_a^*}{C_{t^*}}$$

Calculation of allowed number of cycles N and usage factor D_i

Given the stress $2f_{at^*}^*$ and the number of cycles n, the design number of load cycles to be expected during operation can be calculated.

In principal, two different number of load cycles should be determined. One depending on stress (N_{As}) and the other depending on the load-cycle (N_{Al}).

$$N_{A,s} = \left(\frac{2f_{a,s} - 0.8R_m}{173150 - 0.8R_m}\right)^{-1/0.547}$$

$$2f_{a,s} = 2f_{a,t^*}^* S_s$$

For the determination of the permissible stress range ($2f_{a,s}$), a stress safety factor $S_s = 1.5$ should be used and a load-cycle factor $S_L = 10$ shall be used.

$$N_{A,l} = \left(\frac{2f_{a,l} - 0.8R_m}{173150 - 0.8R_m}\right)^{-1/0.547}$$

$$2f_{a,l} = 2f_{a,t^*}^*$$

After determining N_A, the minimum of the two values should be used for calculating the damage factor. Hence,

$$N = min\left\{N_{A,s}, \frac{N_{A,l}}{S_L}\right\}$$

$$S_L = 10$$

Finally, the damage factor would be:

$$C_i = \frac{n}{N}$$

N_A can also be determined using the following graph:

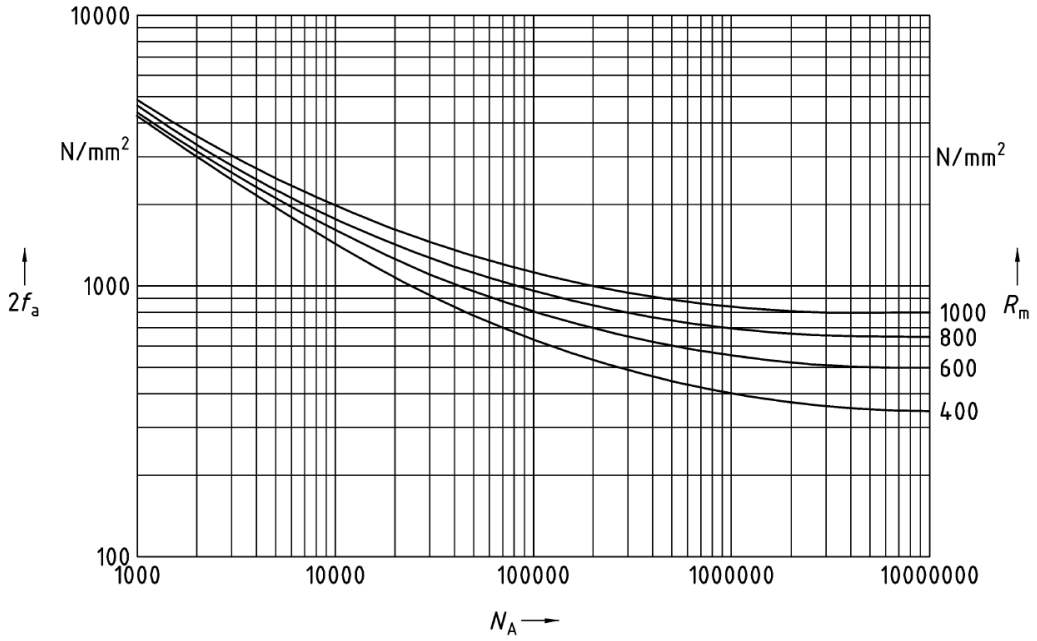

***Figure A - 2**: Number of load cycles for crack initiation as a function of the stress range for unnotched bar specimens of high-temperature ferritic rolled or forged steels at room temperature and f_v=0 (Source: EN12952:3 [14])*

Appendix B: Critical components assessment calculations- Spreadsheets

The following spreadsheets depict the calculations done in accordance with the EN12952-3:2001 code for the fatigue assessment of critical components.

LEGEND		
	Purple Text	Inputs
	Orange Text	Calculations
	Black Text	Label/Description

Component			
HP Drum			
Cycle Data	**Symbol**	**Unit**	
Cycle Type			Cold Start
Calculation Pressure:	pc	N/mm^2	16.2
Calculation Temperature:	tc	°C	349
Operating Pressure:	po	N/mm^2	14.5
min. Cyclic pressure:	pmin	N/mm^2	0.1
max. Cyclic pressure:	pmax	N/mm^2	14.5
min. Cyclic temperature:	tmin	°C	10
max. Cyclic temperature:	tmax	°C	339.6
reference temperature	t*	°C	**257.2**
Material Properties			
material class			SA299 (CC2364)
tensile strength at room temperature	Rm	N/mm^2	522
yield strength at t*	Re(t*)	N/mm^2	250.8
coefficient of linear thermal expansion at t*	βL	1/°C	1.44E-05
modulus of elasticity at t*	E	N/mm^2	188379
thermal diffusivity at t*	Dth	mm^2/s	9.449
Poisson's ratio	v	-	0.3
Component Dimensions			
outside diameter of the component	do	mm	2043
min. wall thickness of the component	ems	mm	107
inside diameter of the component	di	mm	**1829**
mean diameter of the component	dms	mm	**1936**
outside diameter of the branch	dob	mm	390.4
mean wall thickness of the branch	emb	mm	80
inside diameter of the branch	dib	mm	**230.4**

mean diameter of the branch	dmb	mm	310.4
Factors			
water/steam			water
heat transfer coefficient	h	W/m^{2}K	3000
Ck0 (surface finish factor)			1
Ck1 (nozzle group k1 factor)			
Ck2 (nozzle group k2 factor)			
Ck3 (nozzle group k3 factor)			
Ck			
emb/ems	ξ	-	0.7477
zeta	ζ	-	0.4822
alpham	αm	-	2.8240
A		-	0.1273
B		-	0.8211
dmb/dms	z	-	0.1603
alphat	αt	-	1.3826
u0	u0	-	1.1170
gamma	γ	-	-0.3524
W	W	N/mm^2/°C	5.3579
V	V	1/s	-2.34E-03
Assumed Cycle Conditions (dt given)			
dt1 (begin of start-up)	dt1	°C	-85.6
vt1 (begin of start-up)	vt1	°C/s	0.20
dt2 (begin of shut down)	dt2	°C	0
vt2 (begin of shut down)	vt2	°C/s	0.00
Stresses			
Sp,o	Sp,o	N/mm^2	384.95
Sp,min	Sp,min	N/mm^2	2.65
Sp,max	Sp,max	N/mm^2	384.95
St,min	St,min	N/mm^2	-458.63
St,max	St,max	N/mm^2	0
f1	f1	N/mm^2	-455.98
f2	f2	N/mm^2	384.95
CASE (water); if FALSE then magnetite cracking might occur			
IF (Sp,o-po-600)<(Sp,min+St,min)			FALSE
IF (Sp,o-po+200)>(Sp,max+St,max)			TRUE
fv	fv	N/mm^2	-35.51
deltafv	deltafv	N/mm^2	840.93
fv*	fv*	N/mm^2	-35.51
2fva*	2fva*	N/mm^2	840.93
IF (|fv*|+2fva*/2<=Re(t*))			FALSE
2fa*	2fa*	N/mm^2	0
IF (|fv*|+2fva*/2>Re(t*) AND 2fva*<=2Re(t*))			FALSE
fv*	fv*	N/mm^2	0

2fa*	2fa*	N/mm^2	0
IF (2fva*>2Re(t*))			TRUE
2fa*	2fa*	N/mm^2	1409.81
Ct*			0.89
2fa*(t*)	2fa*(t*)	N/mm^2	1580.17
Ss	Ss	-	1.5
2fas	2fas	N/mm^2	2370.25
2faL	2faL	N/mm^2	1580.17
Allowable Cycles			
NAs	NAs	cycles	3622
NAL	NAL	cycles	9347
SL	SL	-	10
N	N	cycles	935
assumed number of cycles	n	cycles	1300
usage factor Di	Ci	-	1.391

Component			
HPSH Outlet Manifold			
Cycle Data	**Symbol**	**Unit**	
Cycle Type			Cold Start
Calculation Pressure:	pc	N/mm^2	16.2
Calculation Temperature:	tc	°C	586
Operating Pressure:	po	N/mm^2	14.25
min. Cyclic pressure:	pmin	N/mm^2	0.1
max. Cyclic pressure:	pmax	N/mm^2	14.25
min. Cyclic temperature:	tmin	°C	10
max. Cyclic temperature:	tmax	°C	567.1
reference temperature	t*	°C	427.825
Material Properties			
material class			SA335 Gr P91
tensile strength at room temperature	Rm	N/mm^2	585
yield strength at t*	Re(t*)	N/mm^2	348.9
coefficient of linear thermal expansion at t*	βL	1/°C	1.34E-05
modulus of elasticity at t*	E	N/mm^2	178664
thermal diffusivity at t*	Dth	mm^2/s	5.795
Poisson's ratio	v	-	0.3
Component Dimensions			
outside diameter of the component	do	mm	273.1
min. wall thickness of the component	ems	mm	50.8
inside diameter of the component	di	mm	171.5

mean diameter of the component	dms	mm	222.3
outside diameter of the branch	dob	mm	114.3
mean wall thickness of the branch	emb	mm	17.1
inside diameter of the branch	dib	mm	80.1
mean diameter of the branch	dmb	mm	97.2
Factors			
water/steam			steam
heat transfer coefficient	h	W/m^2K	1000
Ck0 (surface finish factor)			1
Ck1 (nozzle group k1 factor)			
Ck2 (nozzle group k2 factor)			
Ck3 (nozzle group k3 factor)			
Ck			
emb/ems	ξ	-	0.3366
zeta	ζ	-	0.6468
alpham	αm	-	4.0241
A		-	1.0012
B		-	0.9183
dmb/dms	z	-	0.4372
alphat	αt	-	1.1193
u0	u0	-	1.5924
gamma	γ	-	-0.4219
W	W	$N/mm^2/°C$	3.8280
V	V	1/s	-5.32E-03
Assumed Cycle Conditions (dt given)			
dt1 (begin of start-up)	dt1	°C	-138.7
vt1 (begin of start-up)	vt1	°C/s	0.74
dt2 (begin of shut down)	dt2	°C	0
vt2 (begin of shut down)	vt2	°C/s	0.00
Stresses			
Sp,o	Sp,o	N/mm^2	139.72
Sp,min	Sp,min	N/mm^2	0.98
Sp,max	Sp,max	N/mm^2	139.72
St,min	St,min	N/mm^2	-530.94
St,max	St,max	N/mm^2	0
f1	f1	N/mm^2	-529.96
f2	f2	N/mm^2	139.72
CASE (water); if FALSE then magnetite cracking might occur			
IF (Sp,o-po-600)<(Sp,min+St,min)			FALSE
IF (Sp,o-po+200)>(Sp,max+St,max)			TRUE
fv	fv	N/mm^2	-195.12
deltafv	deltafv	N/mm^2	669.68
fv*	fv*	N/mm^2	-195.12
2fva*	2fva*	N/mm^2	669.68

IF (|fv*|+2fva*/2<=Re(t*))			FALSE
2fa*	2fa*	N/mm^2	0
IF (|fv*|+2fva*/2>Re(t*) AND 2fva*<=2Re(t*))			TRUE
fv*	fv*	N/mm^2	14.06
2fa*	2fa*	N/mm^2	753.51
IF (2fva*>2Re(t*))			FALSE
2fa*	2fa*	N/mm^2	0.00
Ct*			0.69
2fa*(t*)	2fa*(t*)	N/mm^2	1090.03
Ss	Ss	-	1.5
2fas	2fas	N/mm^2	1635.04
2faL	2faL	N/mm^2	1090.03
Allowable Cycles			
NAs	NAs	cycles	9277
NAL	NAL	cycles	29307
SL	SL	-	10
N	N	cycles	2931
assumed number of cycles	n	cycles	1300
usage factor Di	Ci	-	0.444

Component			
RHTR Outlet Manifold			
Cycle Data	**Symbol**	**Unit**	
Cycle Type			Cold Start
Calculation Pressure:	pc	N/mm^2	4
Calculation Temperature:	tc	°C	583
Operating Pressure:	po	N/mm^2	2.98
min. Cyclic pressure:	pmin	N/mm^2	0.1
max. Cyclic pressure:	pmax	N/mm^2	2.98
min. Cyclic temperature:	tmin	°C	10
max. Cyclic temperature:	tmax	°C	566.7
reference temperature	t*	°C	427.525
Material Properties			
material class			SA335 Gr P91
tensile strength at room temperature	Rm	N/mm^2	585
yield strength at t*	Re(t*)	N/mm^2	349
coefficient of linear thermal expansion at t*	βL	1/°C	1.34E-05
modulus of elasticity at t*	E	N/mm^2	178711
thermal diffusivity at t*	Dth	mm^2/s	5.797
Poisson's ratio	v	-	0.3

Component Dimensions			
outside diameter of the component	do	mm	508
min. wall thickness of the component	ems	mm	26.18
inside diameter of the component	di	mm	455.64
mean diameter of the component	dms	mm	481.82
outside diameter of the branch	dob	mm	114.3
mean wall thickness of the branch	emb	mm	8.6
inside diameter of the branch	dib	mm	97.1
mean diameter of the branch	dmb	mm	105.7
Factors			
water/steam			steam
heat transfer coefficient	h	W/m^2K	1000
Ck0 (surface finish factor)			1
Ck1 (nozzle group k1 factor)			
Ck2 (nozzle group k2 factor)			
Ck3 (nozzle group k3 factor)			
Ck			
emb/ems	ξ	-	0.3285
zeta	ζ	-	0.6655
alpham	αm	-	4.0953
A		-	1.0146
B		-	0.9214
dmb/dms	z	-	0.2194
alphat	αt	-	1.4225
u0	u0	-	1.1149
gamma	γ	-	-0.3521
W	W	$N/mm^2/°C$	4.8665
V	V	1/s	-2.40E-02
Assumed Cycle Conditions (dt given)			
dt1 (begin of start-up)	dt1	°C	-55.2
vt1 (begin of start-up)	vt1	°C/s	1.33
dt2 (begin of shut down)	dt2	°C	0
vt2 (begin of shut down)	vt2	°C/s	0.00
Stresses			
Sp,o	Sp,o	N/mm^2	115.28
Sp,min	Sp,min	N/mm^2	3.87
Sp,max	Sp,max	N/mm^2	115.28
St,min	St,min	N/mm^2	-268.63
St,max	St,max	N/mm^2	0
f1	f1	N/mm^2	-264.76
f2	f2	N/mm^2	115.28
CASE (water); if FALSE then magnetite cracking might occur			
IF (Sp,o-po-600)<(Sp,min+St,min)			TRUE
IF (Sp,o-po+200)>(Sp,max+St,max)			TRUE
fv	fv	N/mm^2	-74.74

deltafv	deltafv	N/mm^2	380.04
fv*	fv*	N/mm^2	-74.74
2fva*	2fva*	N/mm^2	380.04
IF (|fv*|+2fva*/2<=Re(t*))			TRUE
2fa*	2fa*	N/mm^2	386.35
IF (|fv*|+2fva*/2>Re(t*) AND 2fva*<=2Re(t*))			FALSE
fv*	fv*	N/mm^2	0.00
2fa*	2fa*	N/mm^2	0.00
IF (2fva*>2Re(t*))			FALSE
2fa*	2fa*	N/mm^2	0.00
Ct*			0.69
2fa*(t*)	2fa*(t*)	N/mm^2	558.55
Ss	Ss	-	1.5
2fas	2fas	N/mm^2	837.82
2faL	2faL	N/mm^2	558.55
Allowable Cycles			
NAs	NAs	cycles	75824
NAL	NAL	cycles	993139
SL	SL	-	10
N	N	cycles	75824
assumed number of cycles	n	cycles	1300
usage factor Di	Ci	-	0.017

Appendix C: Dynamic Simulation Model

MATLAB - SIMULINK model

The following figure shows a print-screen of the dynamic model as it is shown in the MATLAB-Simulink environment.

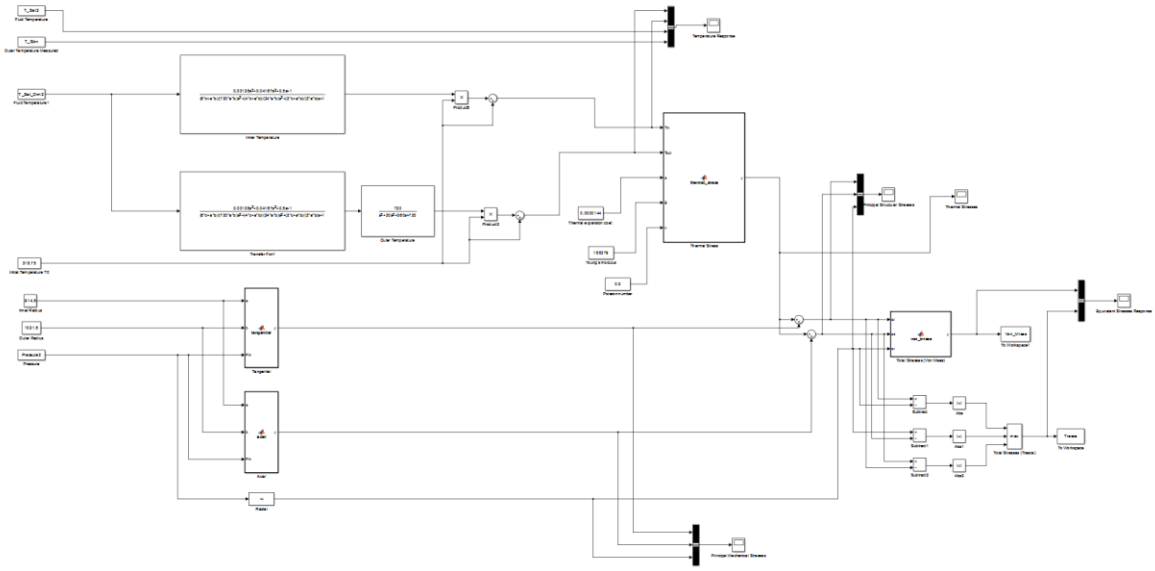

***Figure C - 1**: The dynamic simulation model in the MATLAB-Simulink environment*

Conversion of pressure signal into saturated temperature

The MATLAB code presented in this section is used to convert the measured pressure signal into the saturated temperature using FluidProp.

FluidProp is a software for the calculation of thermophysical properties of fluids. The program is capable of calculating the thermodynamic and transport properties for a large variety of fluids and fluid mixtures using many modern physical models. FluidProp is a software library that complies with the COM standard therefore it can be seamlessly called by many different programs and programming environments. In this study MATLAB is used to call FluidProp.

FluidProp is developed in Delft University of Technology [35].

```
%%%%%%%%%%%%%%%%%%%%%%%%%%%
%      Init_FluidProp      %
%%%%%%%%%%%%%%%%%%%%%%%%%%%

clc

global FP

%Create an instance of the FluidProp COM server
FP = actxserver ('FluidProp.FluidProp');
Msg='FluidProp: COM object created';
```

```
disp(Msg)
%%%FluidProp function to calculate Tsat from pressure%%%
nCmp=1;
Cnc=[1,0];
Cmp='tsat';
Model='IF97';
ErrorMsg=invoke(FP,'SetFluid_M',Model,nCmp,Cmp,Cnc)
P=100; %bar%
q=0; %quality%
Temperature=zeros(size(Pt));
for i=1:size(Pt)
[Temperature(i),ErrorMsg]=invoke(FP,'Temperature','Pq',Pt(i),q);
end
Temperature
```

Rainflow Algorithm

The following MATLAB code is used for implementing the rainflow counting method in a random stress signal. The MATLAB code is obtained online from [30].

```
function rfdemo1(ext)
% function rfdemo1(ext)
%
% RFDEMO1 shows cycles extracted from signal
% using rainflow algorithm.
%
% INPUT:  ext - option, number or vectors with turning
%               points or time history. Default ext=16.
%
% OUTPUT: no enable.
%
% SYNTAX:
%         >>rfdemo1
%         >>rfdemo1(10)
%         >>rfdemo1([2 3 2 4 2 5 1 6])
%

% By Adam Nies³ony
% Revised, 10-Nov-2009
% Visit the MATLAB Central File Exchange for latest version.

error(nargchk(0,2,nargin))

if nargin==0,
    % turning points from 16 random numbers
    ext=sig2ext(randn(4));
elseif length(ext(:))==1,
    % turning points from n random numbers
    ext=sig2ext(randn(1,ext));
else
    % turning points from vector ext
    ext=sig2ext(ext);
end

a=rainflow(ext,1);
[m n]=size(a);

% if n>100,
%     button = questdlg(['Rainflow found ' num2str(sum(a(3,:))) ' cycles!
Do you want to continue?'],...
```

```
%         'Continue Operation','Yes','No','No');
%     if strcmp(button,'No')
%         error('Function aborted by user.')
%     end
% end

col='ymcrgb';
plot(0:length(ext)-1,ext,'k.:')
hold on
wyk=0:0.05:1;
for c=1:n,
    colnr=rem(c-1,6)+1;

    nr1=round(a(4,c)+1);
    nr2=round(a(4,c)+1+a(5,c)*a(3,c));
    if a(3,c)==1.0,
        if ext(nr1)<ext(nr1+1),

plot(wyk.*a(5,c)+a(4,c),cos(pi+wyk.*2*pi)*a(1,c)+a(2,c),col(colnr))
            text(a(4,c),a(2,c)-a(1,c),[int2str(c) '. Cycle, up'],...
                'Color',col(colnr),'VerticalAlignment','top')
        else
            plot(wyk.*a(5,c)+a(4,c),cos(
wyk.*2*pi)*a(1,c)+a(2,c),col(colnr))
            text(a(4,c),a(2,c)+a(1,c),[int2str(c) '. Cycle, down'],...
                'Color',col(colnr),'VerticalAlignment','bottom')
        end
    else
        if ext(nr1)>ext(nr2),
            plot(wyk.*a(5,c)*0.5+a(4,c),cos(
wyk.*pi)*a(1,c)+a(2,c),col(colnr))
            text(a(4,c),a(2,c)+a(1,c),[int2str(c) '. Half-cycle,
down'],...
                'Color',col(colnr),'VerticalAlignment','bottom')
        else

plot(wyk.*a(5,c)*0.5+a(4,c),cos(pi+wyk.*pi)*a(1,c)+a(2,c),col(colnr))
            text(a(4,c),a(2,c)-a(1,c),[int2str(c) '. Half-cycle, up'],...
                'Color',col(colnr),'VerticalAlignment','top')
        end
    end
end
xlabel('peaks, counted from 0')
ylabel('value')
title('Rainflow cycles extracted from signal')
legend('peaks from signal',0)
hold off

disp('Row 1: amplitude')
disp('Row 2: mean')
disp('Row 3: number of cycles (cycle or half cycle)')
disp('Row 4: begin time of extracted cycle or half cycle')
disp('Row 5: period of a cycle')
disp(a)
```

Appendix D: Definition of Physical Properties of Materials

In this section the definition of each physical material property that is used in this study is presented according to [36].

Coefficient of linear thermal expansion

Symbol: a

Units: K^{-1}

The ratio of the change in length to the original length at a reference temperature, T_0, per degree of temperature change, where T_0 is normally room temperature.

Modulus of elasticity

Symbol: E

Units: MPa

The measure of rigidity or stiffness of a material. The ratio of stress below the proportional limit to the corresponding strain or the slope of a stress-strain curve in the range of linear proportionality of stress to strain. Also known as Young's modulus.

Thermal conductivity

Symbol: k

Units: MPa

The quantity of heat transmitted, k, due to unit temperature gradient, in unit time under steady conditions in a direction normal to a surface of a unit area and when the heat transfer is solely dependent on the temperature gradient.

Thermal diffusivity

Symbol: D_{th}

Units: mm^2/s

The constant in the heat conduction equation describing the rate at which heat is conducted through a material. It is linked to thermal conductivity, k, specific heat, C_p, and density ρ through the equation:

$$D_{th} = \frac{k}{\rho C_p}$$

Poisson's ratio

Symbol: ν

Units: (-)

The absolute values of the ratio of transverse (lateral) strain to the corresponding axial strain resulting from uniformly distributed axial stress below the proportional limit of the material.

Bibliography

[1] I. Perez-Arriaga and C. Batlle, "Impacts of intermittent renewables on electricity generation system operation," *Economics of Energy and Environmental Policy,* January 2012.

[2] J. Cox, "Implications of intermittency," *Modern Power Systems,* pp. 22-23, January 2010.

[3] K. Kruger, R. Franke and M. Rode, "Optimization of boiler start-up using a nonlinear boiler model and hard constrains," *Energy,* no. 29, pp. 2239-2251, 2004.

[4] P. Fontaine and J. F. Galopin, "HRSG Optimization for Cycling Duty," *Power Engineering,* 2007.

[5] S. A. Lefton, P. M. Besuner and G. P. Grimsrud, "Understand what it really costs to cycle fossil-fired units," *Coal Power Magazine,* pp. 41-46, March/April 1997.

[6] G. K. Lausterer, "On-line thermal stress monitoring using mathematical models," *Control Engineering Practice,* vol. 5, no. 1, pp. 85-90, 1997.

[7] S. A. Lefton and D. Hilleman, "Make Your Plant Ready for Cycling Operations," *Power Magazine,* August 2011.

[8] S. Lu and B. Wilson, "On-line stress calculation and life monitoring systems for boiler components," in *Transactions of the Institute of Measurement and Control*, 1998.

[9] P. Decoussemaeker and W. P. Bauver, "Asset Management and Condition Monitoring for HRSG's that are Confronted with Increased Cycling," in *The Future of Gas Turbine Technology, 6th International Conference*, Brussels, Belgium, 2012.

[10] V. Birman, "On three-dimensional state of thermal stresses in a transversely isotropic plate with a circular hole," *Int. J. Engineering Sciences,* vol. 33, no. 1, pp. 95-103, 1995.

[11] N. K. Mukhopadhyay, B. K. Dutta and H. S. Kushwaha, "On-line fatigue-creep monitoring system for high-temperature components of power plants," *International Journal of Fatigue,* vol. 23, pp. 549-560, 2001.

[12] K. Maile, H. Purper, B. Wilson, K. Rohler, H. Lehmann, J. Garcia and J. Fernandez, "A new monitoring system for piping systems in fossil fired power plants," *Int. J.*

Pres. Ves. & Piping , vol. 66, pp. 305-317, 1996.

[13] S. Bracco, "Dynamic simulation of combined cycles operating in transient conditions: an innovative approach to determine the steam drums life consumption," in *The 25th International Conference on Efficiency, Cost, Optimization, Simulation and Environmental Impact of Energy Systems*, Perugia, Italy, 2012.

[14] "EN12952 (2001) "Water-tube boilers and auxiliary installations - Part 3: Design and calculation for pressure parts; Part 4: In-service boiler life expectancy calculations"," CEN, Brussels.

[15] J. B. Kitto and S. C. Stultz, Steam/its generation and use, Ohio: The Babcock & Wilcox Company, 2005.

[16] J. F. Harvey, Theory and Design of Pressure Vessels, New York: Van Nostrand Reinhold, 1991.

[17] M. A. Miner, "Cumulative Damage in Fatigue," *Journal of Applied Mechanics,* vol. 12, pp. A-159, September 1945.

[18] J. Taler, B. Weglowski, W. Zima, S. Gradziel and M. Zborowski, "Analysis of Thermal Stresses in a Boiler Drum During Start-Up," *Journal of Pressure Vessel Technology,* vol. 121, no. 1, pp. 84-93, 1999.

[19] J. F. Harvey, Theory and design of pressure vessels, New York: Van Nostrand Reinhold, 1991.

[20] S. Bracco, "Simulation Models of Steam Drums Based on the Heat Transfer Equations," *Applied Mathematical Sciences,* vol. 4, no. 74, pp. 3687-3712, 2010.

[21] T. S. Kim, D. K. Lee and S. T. Ro, "Analysis of thermal stress evolution in the steam drum during start-up of a heat recovery steam generator," *Applied Thermal Engineering,* vol. 20, pp. 977-992, 2000.

[22] A. Kandil, A. A. El-Kady and A. El-Kafrawy, "Transient thermal stress analysis of thick-walled cylinders," *Int. J. Mech. Sci ,* vol. 37, no. 7, pp. 721-732, 1995.

[23] A. Kandil, "Analysis of thick-walled cylindrical pressure vessels under the effect of cyclic internal pressure and cyclic temperature," *Int. J. Mech. Sci.,* vol. 38, no. 12, pp. 1319-1332, 1996.

[24] X.-K. Zhu and B. N. Leis, "Average shear stress yield criterion and its application to plastic collapse analysis of pipelines," *Pressure Vessels and Piping,* no. 83, pp. 663-671, 2006.

[25] A. Nieslony, "Determination of fragments of multiaxial service loading strongly

influecting the fatigue of machine components," *Mechanical Systems and Signal Processing,* no. 23, pp. 2712 - 2721, 2009.

[26] D. F. Socie, "Fatigue-life prediction using local stress-strain concepts," *Experimental Mechanics,* vol. 17, no. 2, pp. 50-56, 1977.

[27] "ASTM E 1049-85, Standard Practices for Cycle Counting in Fatigue Analysis," 1997.

[28] Y.-L. Lee, J. Pan, R. B. Hathaway and M. E. Barkey, Fatigue Testing and Analysis - Theory and Practice, Elsevier, 2005.

[29] S. D. Downing and D. F. Socie, "Simple rainflow counting algorithms," *International Journal of Fatigue,* pp. 31-40, 1982.

[30] A. Nieslony, "Rainflow counting method, set of functions with user guide for use with MATLAB," 2010. [Online]. Available: http://www.mathworks.com/matlabcentral/fileexchange/3026.

[31] D. Roylance, "Fatigue," MIT, Department of Materials Science and Engineering, Cambridge, MA 02139, 2001.

[32] H. E. Boyer, Atlas of Fatigue Curves, ASM International, 1986.

[33] C. Bathias, "There is no infinite fatigue life in metallic materials," *Fatigue Fract Engng Mater Struct ,* vol. 22, pp. 559-565, 1999.

[34] ALSTOM, "Lifetime Assessment of Key HRSG Components".

[35] P. Colonna and T. van der Stelt, *FluidProp: a program for the estimation of thermo physical properties of fluids,* Energy Technology Section, Delft University of Technology, 2004.

[36] EPRI, "Carbon Steel Handbook," Palo Alto, CA, 2007.

[37] B. S. Ouwerkerk, "Dynamic Modeling of an Industrial Scale Heat Recovery Steam Generator, MSc Thesis," Delft, 2011.

[38] "MatWeb Material Property Data," [Online]. Available: http://www.matweb.com/search/DataSheet.aspx?MatGUID=89da5370958c405fa2463ec3a3f250ac&ckck=1.